Translational Oncology 37 (2023) 101760

Contents lists available at ScienceDirect

Translational Oncology

journal homepage: www.elsevier.com/locate/tranon

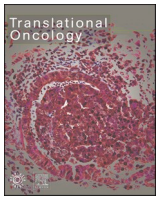

Stochastic epithelial-mesenchymal transitions diversify non-cancerous lung cell behaviours

Sugandha Bhatia [a,*], Jennifer H Gunter [a,b], Joshua T Burgess [a], Mark N Adams [a], Kenneth O'Byrne [a,c], Erik W Thompson [a], Pascal HG Duijf [a,d,e,f,*]

[a] Queensland University of Technology (QUT), School of Biomedical Sciences, Centre for Genomics and Personalised Health at the Translational Research Institute, Woolloongabba 4102, QLD, Australia
[b] Australian Prostate Cancer Research Centre-Queensland (APCRC-Q), Queensland University of Technology, Woolloongabba 4102, Australia
[c] Princess Alexandra Hospital, Woolloongabba 4102, QLD, Australia
[d] Centre for Cancer Biology, Clinical and Health Sciences, University of South Australia and SA Pathology, Adelaide SA, 5001, Australia
[e] Institute of Clinical Medicine, Faculty of Medicine, University of Oslo, Oslo, Norway
[f] Department of Medical Genetics, Oslo University Hospital, Oslo, Norway

ARTICLE INFO

Keywords:
Clonal diversity
Epigenetics
Epithelial-mesenchymal transition (EMT)
Epithelial-mesenchymal plasticity (EMP)
Intra-tumour heterogeneity
Metabolic reprogramming

ABSTRACT

Epithelial-mesenchymal plasticity (EMP) is a hallmark of cancer. By enabling cells to shift between different morphological and functional states, EMP promotes invasion, metastasis and therapy resistance. We report that near-diploid non-cancerous human epithelial lung cells spontaneously shift along the EMP spectrum without genetic changes. Strikingly, more than half of single cell-derived clones adopt a mesenchymal morphology. We independently characterise epithelial-like and mesenchymal-like clones. Mesenchymal clones lose epithelial markers, display larger cell aspect ratios and lower motility, with mostly unaltered proliferation rates. Stemness marker expression and metabolic rewiring diverge independently of phenotypes. In 3D culture, more epithelial clones become mesenchymal-like. Thus, non-cancerous epithelial cells may acquire cancer metastasis-associated features prior to genetic alterations and cancerous transformation.

Introduction

Human cancer presents a major health and economic burden and amongst different cancers the most predominant cause of mortality and morbidity worldwide is lung cancer [1]. Early insights into the study of tumour progression and heterogeneity points to genomic instability resulting from mutations in viral-associated genes, including oncogenes, tumour suppressor genes and chromosomal karyotypic changes [2,3]. However, the non-genetic heterogeneity of cancer, contributed by various environmental, cancer microenvironment, epigenetic and host factors, also plays a key molecular role in adding complexity to cancer pathogenesis and treatment response [4,5]. Thus, understanding key insights into cancer heterogeneity and clonal dynamics is important for the advancement of cancer research. Also, this cancer heterogeneity imparts clinical relevance as clonal diversity within the cancer influences metastatic potential, therapeutic response and patient survival [6]. These clonal and subclonal cancer diversities and dynamics are thought to be influenced by cellular heterotypic stimuli, including hypoxia, spatial proximity, clonal frequency, and cellular plasticity [7–9]. Therefore, characterising and identifying the mechanisms underlying this non-genetic heterogeneity is also of fundamental clinical importance for guiding treatment modalities and avoiding tumour recurrence.

The functional consequences of non-genetic tumoral heterogeneity are also attributed to phenotypic plasticity around epithelial-mesenchymal transition (EMT). EMT, a fundamental and quintessential process for embryonic development and tissue healing, is dysregulated during tumour growth, cancer cell dissemination, immune escape and activation, and metastasis [10–13]. The original concept of binary switching between two well-characterised, isogenic, epithelial and mesenchymal phenotypic states within a tumour was recently challenged with the advent of subset enrichment [14], single-cell RNA-sequencing [15,16], spatial profiling [17] and molecular barcoding techniques [18]. These technologies have revealed that cellular plasticity manifests as intermediate states, or along a continuum of hybrid epithelial-mesenchymal (E-M) states [19–21]. Thus, the

* Corresponding author.
E-mail addresses: s3.bhatia@qut.edu.au (S. Bhatia), pascal.duijf@unisa.edu.au (P.H. Duijf).

https://doi.org/10.1016/j.tranon.2023.101760
Received 15 May 2023; Received in revised form 23 July 2023; Accepted 7 August 2023
Available online 21 August 2023

well-acknowledged term epithelial-mesenchymal plasticity (EMP) [12] encompasses the bidirectional axis of phenotypic change through distinct trajectories and states, including epithelial-mesenchymal transition (EMT), partial, hybrid (E/M) or quasi-mesenchymal states and the reverse process of mesenchymal-epithelial transition (MET) [22]. When confronted with chemo- and immuno-therapies, this EMP source of non-genetic heterogeneity enables the tumour to undergo reversible and transient changes [23–28]. Of particular importance are the implications of EMP for immune sensitivity and resistance, with hybrid and quasi-mesenchymal states showing increased expression of immune checkpoints [28,29]. Recent studies are also appreciating the impact of EMP on cancer stem cells [30] and circulating tumour cells [31,32] and observing that the hybrid-EM phenotype confers the carcinoma cells with stemness potential [33], greater metastatic competence in the form of circulating tumour cell clusters [34–39], and therapy resistance [40]. Cancer stem cells have also been implicated in cancer progression to impart cancer with functional heterogeneity for survival and drug resistance [41]. Moreover, stochastic cell state transitions can also result in stemness traits and can fuel further aggressive tumour characteristics and heterogeneity [42].

There are currently limited studies that focus on how phenotypic plasticity differs between many cancer cell clones within a single isogenic population [17,43–45] because this attribute has mostly been studied in populations of cancer cells which possess genetic heterogeneity and chromosomal aneuploidy [46]. Moreover, as it is a hallmark of cancer, EMP is typically studied in cancer cells, rather than in non-cancerous cells. Thus, modelling heterogeneity in both cancer and non-cancer cells in relation to cellular plasticity and functional heterogeneity in experimental and pre-clinical settings is fundamental to the understanding of cancer evolution in the context of treatment strategies. In addition, metabolic reprogramming is an emerging essential hallmark mechanism for tumour progression [47]. Metabolic flux between oxidative phosphorylation (OXPHOS) and aerobic glycolysis, termed the Warburg Effect, optimises ATP synthesis and enhances biomass synthesis while balancing the levels of reactive oxygen species (ROS) [48].

The study herein investigated a panel of single-cell clones generated in the near-diploid human bronchial epithelial cell line, HBEC-3KT, to create non-cancerous and genetically homogeneous clones. Genetically heterogeneous HBECs triggered with oncogenic manipulations targeting *Kras* mutation, *p53* knockdown along with cMyc overexpression have been studied for EMT induction [49] and the *ZEB1* transcription factor has been found to induce EMT in this transformation model [50]. Further, HBEC-3KT as a non-malignant lung culture model also exhibited altered EMT markers when exposed to cigarette smoke condensate carcinogens [51]. However, systematic characterization of clones generated from a non-transformed immortalized cell line for their functional trait signals the presence of only non-genetic heterogeneity is limited in terms of studying intrinsic phenotypic plasticity. Our systematic characterisation of clones included analyses of both genetic and phenotypic heterogeneity via SNP arrays, cell morphology assessment, determination of doubling time, migration speed, assessment of various EMT markers at the transcriptional level, and protein expression and localization analyses of the mesenchymal and epithelial markers, respectively vimentin and EpCAM. Real-time bioenergetics analyses and stemness marker expression were also conducted for the clones and parental HBEC-3KT cells, revealing clonal diversity. This integrated retrospective analysis thus reflects the specific functional attributes of the single cell-generated clones, and how they correlate amongst and within the classified groups of parental-like and mesenchymal classes.

Materials and methods

Cell lines and cell culture

HBEC-3KT, immortalized human bronchial epithelial cells were established previously by introducing mouse Cdk4 and human TERT into normal, primary human bronchial epithelial cells. Cells were a gift from Professor John D Minna, University of Texas Southwestern Medical Centre, USA [52]. HBEC-3KT cells were cultured with KSFM media (Life Technologies Inc., Carlsbad, CA) containing 50 μg/mL of Bovine Pituitary Extract (BPE) (Life Technologies Inc.) and 5 ng/mL of EGF (epidermal growth factor) (Life Technologies Inc.) supplemented with 10% foetal bovine serum (FBS; Gibco™, Thermo, Victoria, Australia) and 1% antibiotics, penicillin and streptomycin (Gibco™, Life Technologies catalogue number—15,140,122). Cell number and viability were routinely determined using 0.4% trypan blue dye exclusion and loaded onto the TC20™ Automated Cell counter (Bio-Rad). Cells were routinely confirmed negative for *Mycoplasma* (MycoAlert™ mycoplasma detection kit, Lonza catalogue number LT07–318). To assess organoid behaviours of the parental HBEC-3KT parental cells and clones, 70 μl undiluted EHS Matrix Extract (Sigma-Aldrich) was coated on 48 well-plates and cells were allowed to set for 30–45 min. Once set, 100 μl diluted (4% vol/vol in chilled distilled water) EHS was placed on the surface of the set EHS, followed by 300 μl of media containing 10^5 HBEC-3KT parental cells or derived clones.

Single-cell cloning

Single-cell sorting was carried out in 96-well plates from trypsinized cells using the limiting dilution technique. The wells were microscopically examined and marked to ensure single cells were seeded per well across three 96-well plates. Wells were propagated to generate single-cell clones in equal proportions of media with HBEC-3KT cell-conditioned media. Conditioned media was sourced from 5-day old cultured HBEC-3KT cells and was double-filtered prior to its use. Plates were maintained at 37 °C in a 5% (v/v) CO_2-humidified atmosphere and were examined every week for the presence of single colonies. Depending on the proliferation density of the expanded colonies, selected clones were expanded to 24-well plates via Passage 1 in the conditioned media, 6-well plate via Passage 2 and then into T25 flasks via Passage 3 in the HBEC-3KT media, and subsequently cryopreserved (Fig. 1A). In addition to the parental HBEC-3KT cells, 8 selected clones were profiled further for their genetic, functional and molecular traits, as described below. Morphological assessment of the clones and parental cells was performed using an Olympus CKX41 inverted microscope and by Crystal Violet staining [53].

Karyotype analysis

Genomic DNA was prepared from 5×10^6 cells with the DNeasy Blood and Tissue Kit (Qiagen) and submitted to the Australian Translational Genomics Centre (ATGC) at Queensland University of Technology (QUT) and Princess Alexandra Hospital. To identify whether stochastic/spontaneous aneuploidies or chromosomal rearrangements arose while propagating single-cell clones, SNP array analyses were performed for all clones and the parental HBEC-3KT cell line to compare copy numbers across the genome. Specifically, DNA was normalised to 50 ng per μL based on submitted Qubit concentrations. Four microlitres of normalised DNA was genotyped on Illumina Infinium™ Global Screening Array-24+MD v3.0 (Illumina, 20,030,774) as per manufacturer 's instructions. The arrays were scanned on an Illumina iScan system and the raw fluorescence intensity data was normalized and clustered for each sample using Illumina Genome Studio software (Illumina version 2.0.5). Genome-wide copy number alterations (CNAs) were determined using the *cnvPartition* algorithm (Illumina version 3.2.0) based on the log R ratios (LRRs) for single nucleotide polymorphisms (SNPs).

RNA extraction, cDNA synthesis and reverse transcriptase-quantitative PCR (RT-qPCR)

Total RNA was extracted from cells using TRIzol (Life Technologies)

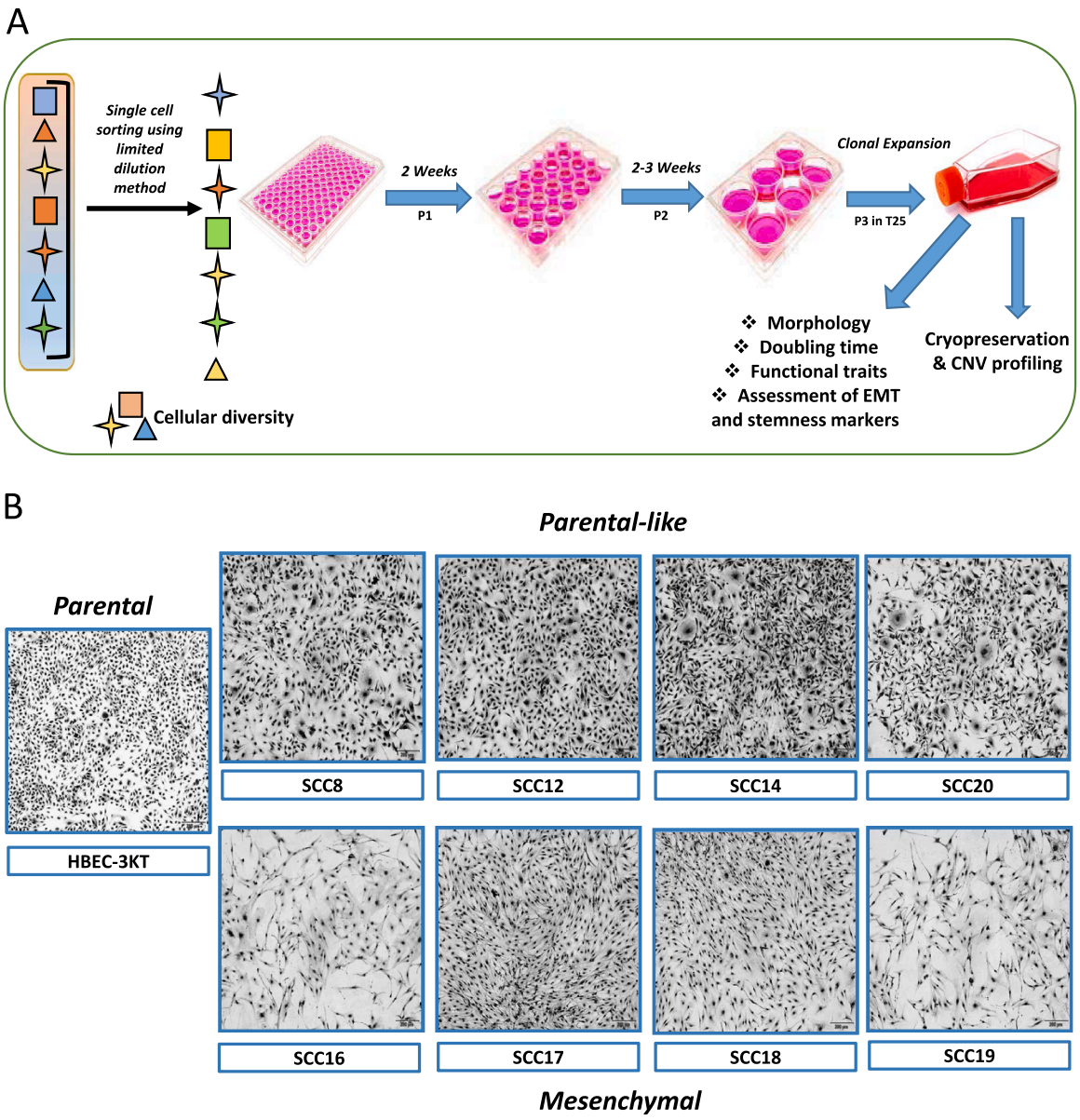

Fig. 1. Phenotypic heterogeneity of single cell-derived clones of HBEC-3KT (A) Schematic representation of the single-cell clone generation, characterisation and cryopreservation. P1-P3 refer to passage numbers 1–3. See main text for detailed description. (B) Bright-field images of crystal violet-stained parental HBEC-3KT cells and distinct clones grouped based on their morphologies, characteristic as either epithelial/parental-like (top four) or mesenchymal phenotype with elongated spindle-like shapes (bottom four). Scale bars, 200 μm.

and subsequent reactions were carried out as per the Bioline Isolate II RNA Micro kit manufacturer's instructions. cDNA was synthesized using the SensiFAST™ cDNA Synthesis kit from Bioline. RT-qPCR was performed using the SYBR Green Master Mix in a ViiA7 Real-Time PCR system (Applied Biosystems, Carlsbad, CA, USA) and analysis performed using Quantstudio™ Real-Time PCR software v1.1 (Applied Biosystems, Life Technologies). The primer sequences are listed in Supplementary Table S1. The thermal cycling condition were as follows: pre-denaturation at 95 °C for 10 min (Ramp Rate – 1.6 °C/sec) for one cycle, 40 cycles of denaturation at 95 °C for 15 s and annealing at 60 °C for 90 s (Ramp Rate – 1 °C/sec). Data were normalized against the overall mean expression of all measured genes [54] or normalized with the average CT value of the "housekeeping gene" RPL32 . The results were calculated using either of the two methods, as indicated, and presented as fold changes.

Immunofluorescence

The parental HBEC-3KT cells and the single cell-derived clones were seeded at a density of 10,000 cells/well in 96-well glass-bottomed, black-walled plates (CellVis, Mountain View, CA, Cat. #P96–1.5H–N). For immunocytochemistry, the growth medium was discarded, and cells were washed twice gently with Dulbecco's modified phosphate-buffered saline (DPBS; pH 7.5). Briefly, cells were fixed and permeabilized in 4% paraformaldehyde + 0.1% Triton X-100, rinsed with DPBS, and incubated with the designated primary antibodies at 4 °C overnight. After rinsing in DPBS, cells were incubated for 2 h at room temperature in the dark on a gentle rotary shaker with appropriate fluorescence-conjugated secondary antibody (Supplementary Table S2) and with diamidino phenyl indole (DAPI) as a nuclear stain (diluted to a final concentration of 1 μg/mL). The plates were then washed twice with DPBS and images captured on a high-content imaging platform InCell analyser 6500HS (GE Healthcare, Buckinghamshire, UK) with approximately 5 fields of

view taken per well. Images were projected and processed with Fiji and analysed for marker intensity quantification using the InCell Investigator software IN Carta analysis software v1.14 (GE Healthcare).

Flow cytometry

Cells were harvested with Accutase® (Corning, catalogue # 25–058-CI) and stained with anti-human CD44-FITC (BD Pharmingen, catalogue #555,478) and anti-human CD24-PB (Exbio, catalogue # PB-503-T100) antibodies, as per manufacturer-recommended dilutions for 1 hour at room temperature on a rotary shaker. Cells were analysed in the presence of propidium iodide (1 μg/mL) using a BD LSR Fortessa (BD Biosciences). After doublet discrimination and compensation for spectral overlap, samples were analysed using FlowJo Software v10.0.7 (BD Biosciences).

Livecyte® migration and invasion assay

For live-cell imaging, experiments were performed on the Livecyte platform (Phasefocus, Sheffield, UK). Cells were seeded in 48-well plates or 96-well glass bottom plates at a density of 10,000 cells/well. Images were acquired every 30 mins at 37 °C over a period of 72 h on an imaging system at 10X magnification. Imaging was performed on two to four regions of interest (ROI) from each well with selected surface areas of either 750×750 μm or 1000×1000 μm. The images were compiled into videos using Livecyte software and the data was analysed using the Livecyte Cell Analysis toolbox supplemented with the separate dashboards for morphology and random motility outputs. Cells ($n \approx 50$) from each sample were also manually tracked to scan cytokinesis of cells to two daughter cells to their next cytokinesis to determine exact cell doubling times.

Seahorse ATP rate assay measurement

Seahorse cell culture plates (Seahorse Bioscience, 102601–100) were coated overnight with poly-L-ornithine and were seeded at a density of 20,000 cells per well (XFe96 cell culture microplate; Seahorse Biosciences, North Billerica, MA, USA). The cells were allowed to grow for 24–48 hours at 37 °C in 5% CO_2, after which media was aspirated, cells were washed and fresh assay media added (unbuffered DMEM, supplemented with 10 mM glucose, 1 mM sodium pyruvate, 2 mM L-glutamine at pH 7.4). The cells were incubated for 1 hour at 37 °C in a non-CO_2 incubator. Mitochondrial complex inhibitors (1.5 μM oligomycin and combined 1 μM rotenone with 1 μM antimycin A) were preloaded in the injection ports. For ATP rate assay, contributions from mitochondria and glycolytic for the metabolic flux measurements were assessed with XF Wave software (Seahorse Bioscience, Agilent). Experiments were performed in triplicates and the data were normalized to cell numbers.

Statistical analysis

All experiments were carried out at least three times unless otherwise indicated. Data were analysed using GraphPad Prism version 9.5 statistical software (GraphPad Software, La Jolla, CA, USA). Data is represented as mean ± standard deviation. Unpaired two-tailed student's *t* tests were used for comparisons between two groups and one-way ANOVA were used for comparisons of more than two groups. *P* values lower than 0.05 were considered statistically significant.

Results

Lung epithelial single-cell clones acquire phenotypic heterogeneity without genetic diversity

We derived single-cell clones (SCCs) from the HBEC-3KT immortalized normal human bronchial epithelial cell line (Fig. 1A; see Methods). Eight single cell-derived clonal populations were thoroughly characterised to study the clonal diversity and heterogeneity. During propagation of the clones, bright-field microscopic scanning clearly depicted a change in the cellular morphology for several of the clones. Based on crystal violet staining, we classified the four selected clones which closely resemble the epithelial morphology of the parental line (SCCs 8, 12, 14 and 20) as 'parental-like' (Fig. 1B, top panels). In contrast, we selected four other clones (SCCs 16–19), whose crystal violet staining clearly revealed distinct elongated and spindle-like morphologies and classified these as 'mesenchymal' SCCs (Fig. 1B, bottom panels). Altogether, of the 25 SCCs whose morphologies we analysed, 11 (44%) of SCCs had retained a parental-like morphology, whereas 14 (56%) had adopted a mesenchymal phenotype. This indicates that an EMT-like morphological change is common amongst non-cancerous HBEC-3KT lung cells.

We undertook genome-wide SNP array profiling of the parental cells and all 8 derived clones to examine whether they exhibited any chromosomal or focal copy number variations. The parental HBEC-3KT cells exhibit a near-diploid karyotype, harbouring 3 copies of chromosome 5 and 20q arm, as observed previously [52], and 20p loss. Comparison of the copy number variation (CNV) profiles of the parental-like cells to those of the mesenchymal clones did not reveal any overt differences in their ploidy representation (Supplementary Fig. 1). The data analysed showed no apparent genetic differences between the parental cells and the 8 SCCs. Since the cells were also cultured under identical conditions, we conclude that a majority of non-malignant lung epithelial cells stochastically adopt mesenchymal morphologies under the same environmental conditions without underlying genetic alterations.

Epithelial-mesenchymal plasticity exists across single cell-derived clones

To assess the heterogeneity between the HBEC-3KT parental cells and single-cell clones at gene expression level, we determined the expression levels of 26 selected genes, including genes encoding canonical epithelial and mesenchymal markers and associated transcription factors, stemness markers, growth factor receptors, as well as 10 selected integrin family genes.

Compared to parental HBEC-3KT cells the gene expression heatmap for selected EMT canonical markers displayed strong downregulation of the epithelial-associated genes *EPCAM* (range 85 to 323-fold), *GRHL2* (3.8 to 6.7-fold), *CK19* (7 to 19-fold) in all mesenchymal clones (SCC16, SCC17, SCC18 and SCC19) (Fig. 2A). Concomitantly, the mesenchymal clones display upregulation of the mesenchymal-associated genes *CDH2* (N-cad; 2 to 5-fold) and *MMP-2* (3.3 to 7-fold). While evaluating EMT transcription factor expression, the levels of *ZEB1* and *TWIST1* were higher in all mesenchymal clones, whereas no robust expression level changes were seen for the EMT-associated transcriptional regulators *SNAI1* or *FOXA1* in the mesenchymal clones, as compared to the HBEC-3KT parental cells. Amongst the evaluated stemness markers, *NANOG* was overexpressed in three out of the four mesenchymal clones (range 2.8 to 6.8-fold), whereas *CD24* expression was 2 to 3-fold lower in all mesenchymal clones in comparison to the parental cells.

Gene expression levels of the growth factor receptors *EGFR* and *HER2* (*ERBB2*) did not change considerably amongst any of the clones (Fig. 2A). However, we observed a markedly increased upregulation of *TGFBR2* expression by more than 4-fold and up to 7.3-fold in all SCCs, except SCC12, irrespective of their parental-like and mesenchymal phenotype. Also, the expression levels of BMP-7, which counter-regulates TGFβ-Smad signalling [55], were downregulated in many clones. The unsupervised hierarchical clustering of the gene expression changes in the clones relative to the parental cells also clusters mesenchymal clones closely together, while, separately, parental-like clones, including SCC12, cluster together with the parental cells.

Integrins play a key role in cell-cell interactions and cell migration in the tumour microenvironment. Therefore, we also determined the gene expression levels of integrin subunits α1, α2, α6, α10, β1, β3, β4, β5 and

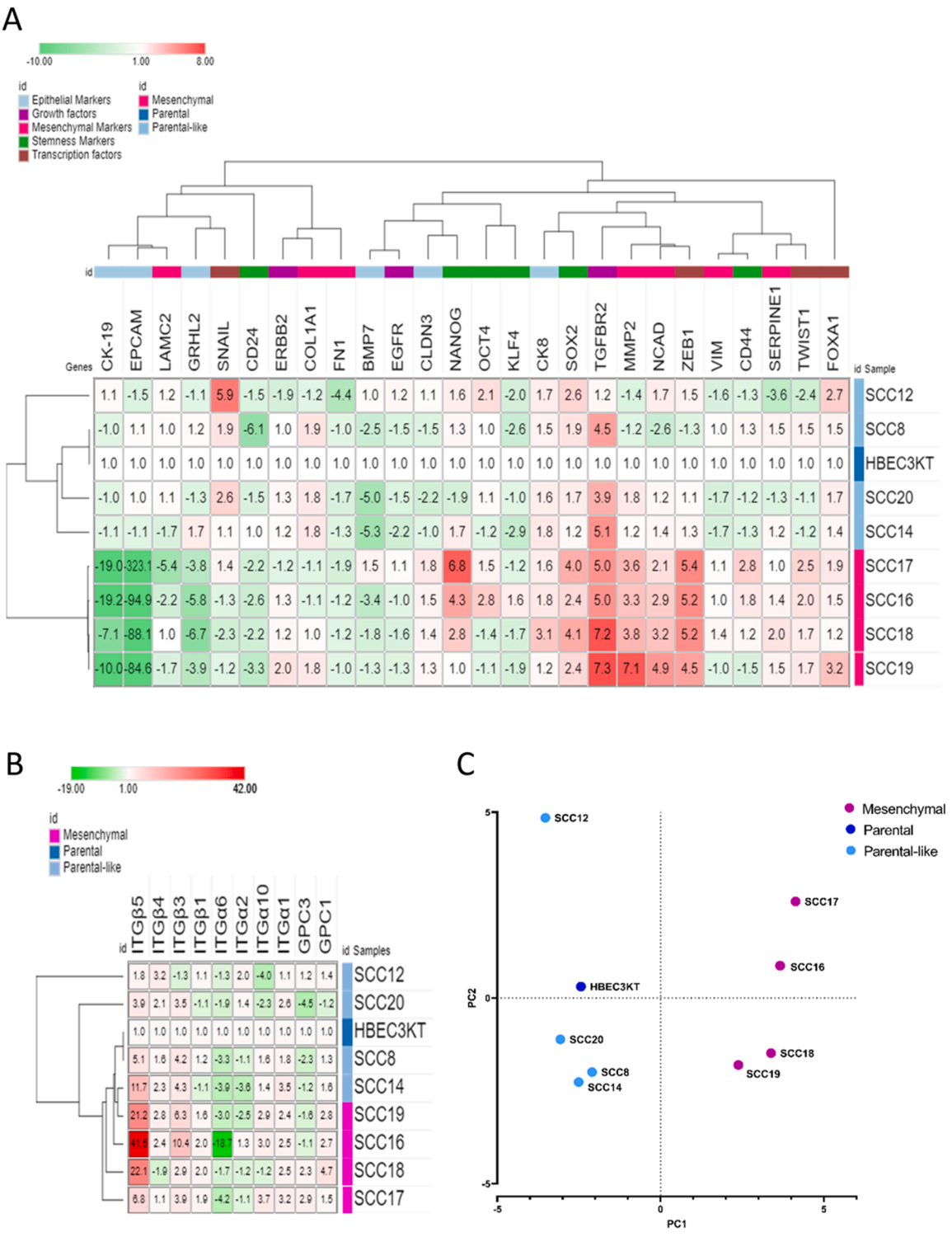

Fig. 2. EMP-associated changes reflected in gene expression profiles of mesenchymal HBEC-3KT clones (A) Heat map showing 26 gene panel expression profiles in HBEC-3KT parental cells and single cell-derived clones. Hierarchical unsupervised clustering was performed using one minus Pearson correlation for the samples. For each sample, the colour annotation is shown above the heatmap. These reflect the cellular morphology types and gene expression categories. Genes are categorised as epithelial-associated (*EpCAM, CK-8, CK-19, GRHL2, BMP7, CLDN3*), mesenchymal-associated (*N—CAD, VIM, FN1, COL1A1, LAMC2, SERPINE1, MMP-2*), growth factor receptors (*ERBB2, EGFR, TGFBR2*), stemness markers (*CD44, CD24, OCT4, NANOG, SOX2, KLF4*) and EMT-inducing transcription factors (*ZEB1, Snail, TWIST1, FOXA1*). (B) Heat map showing 10 gene panel expression profiles for integrin gene family. Hierarchical unsupervised clustering was performed within Morpheus using one minus Pearson correlation for the samples. (C) Principal Component Analysis of all 26 epithelial-mesenchymal genes panel evaluated between clones and HBEC-3KT parental cells using RT-qPCR.

β6 and glypican (GPC1, GPC3) in the HBEC3KT parental cells and derived SCCs (Fig. 2B). Although the expression of glypicans GPC1 shows an upward expression trend in all the mesenchymal clones and GPC3 expression showed an upregulation in two of the mesenchymal clones (SCC17, SCC18) and downregulation in two of the parental-like clones (SCC8 and SCC20), the expression of integrins showed overall variable responses in parental-like and mesenchymal clones. The expression of integrin β1 was upregulated by an average of 1.5–2-fold in all the mesenchymal clones. The expression of integrin β3 and β5 was upregulated in 7 out of 8 clones (except SCC12), although the expression of integrin β5 was much higher in mesenchymal clones. Although the expression of integrin α3 was found to be lower in parental and all clones

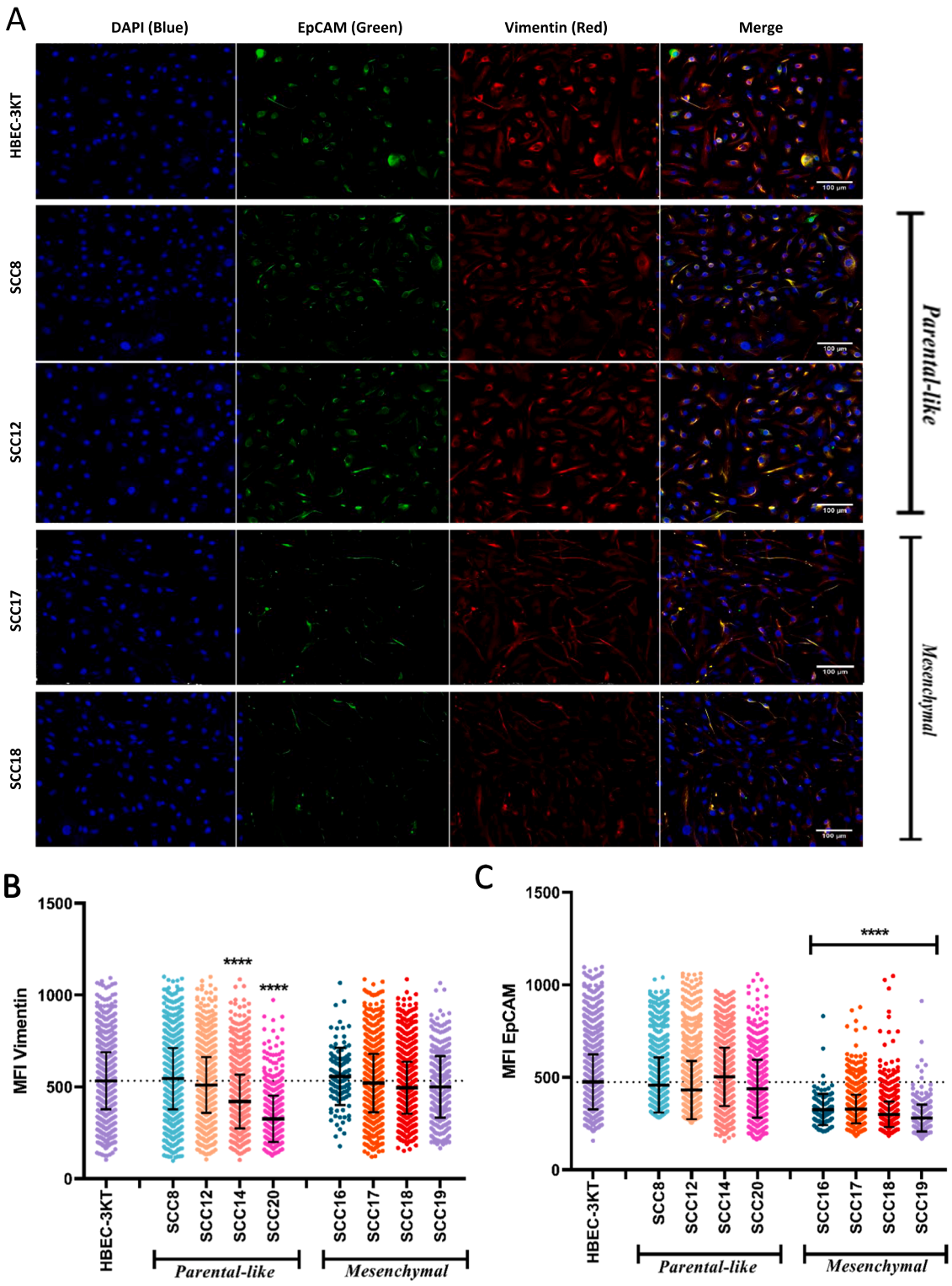

Fig. 3. Immunofluorescence microscopy analysis of changes in the expression levels of EMT marker proteins. (A) Parental HBEC-3KT cells and the selected clones were stained with antibodies against the epithelial marker EpCAM or the mesenchymal marker vimentin. Scale bars, 100 µm. Staining intensity of (B) EpCAM and (C) vimentin for the parental HBEC-3KT cells and clones were assessed using IN Carta using median fluorescence intensity (MFI). Significant differences were calculated by one-way ANOVA and non-parametric Dunnett's multiple comparisons test. **** $P < 0.0001$.

of HBEC3KT, the expression of integrin α2 and α6 was downregulated in many clones of HBEC3KT as compared to parental cells (Fig. 2B). Overall, the differences in integrin gene expression are variable between epithelial and mesenchymal SCCs. Nonetheless, unsupervised hierarchical clustering based on integrin gene expression alone also clusters parental and parental-like clones together and, separate from these, mesenchymal clones together (Fig. 2B).

Taken together, the divergent epithelial and mesenchymal morphologies that we observed correlate strongly with the up- and down-regulation of established epithelial and mesenchymal marker genes (Supplementary Fig. 2A).

Next, we performed principal components analysis (PCA). This demonstratesthat the clones that we characterised as mesenchymal based on their morphology (Fig. 1B) (labelled SCC16, SCC17, SCC18 and SCC19) cluster as a separate group, whereas parental-like clones (SCC8, SCC14, SCC20) overlap with HBEC-3KT parental cells (Fig. 2C). While the first principal component (PC1) of clone SCC12 is similar to the parental and these parental-like clones, PC2 clustered it into a position separate from the parental cells, reflecting subtle but distinct changes in its transcriptional repertoire (Fig. 2C). These data indicate that the derived clones with the mesenchymal traits embark on trajectories distinct from both the parental line and SCCs that retain an epithelial morphology.

HBEC-3KT clonal heterogeneity of distinct epithelial and mesenchymal markers is observed at the protein level

Since EpCAM mRNA levels were strongly downregulated in the mesenchymal clones, we sought to examine whether differential expression between the parental-like and mesenchymal-like clones for the EpCAM expression could be validated at the protein level. Immunofluorescence staining for the markers EpCAM and vimentin was performed to precisely delineate the spatial localization and expression of these EMP status markers across the different HBEC-3KT clones. HBEC-3KT cells and all clones were positive for vimentin expression across cell populations. However, the fluorescence intensity markedly differed for two of the parental-like clones (SCC-14 ($p < 0.0001$), SCC-20 ($p < 0.0001$)) which displayed significantly less intensity distribution for vimentin expression as compared to the parental cells (Fig. 3A and B).

Correlating with our RT-qPCR results for EpCAM gene expression, the number and intensity distribution of EpCAM-positive cells were significantly lower for all mesenchymal clones as compared to the parental cells ($p < 0.0001$) (Fig. 3A and C). There were also subtle differences between the parental cells and parental-like clones in comparison to mesenchymal clones in the cytoskeletal shape and arrangement of cell size, as depicted by the vimentin staining (Fig. 3A). Since all the HBEC-3KT cells and derived SCCs express vimentin, these findings indicate that the parental cells and the parental-like clones represents a quasi-mesenchymal-like or a hybrid EMT state, whereas the mesenchymal clones obtained from the single cell clonal expansion exhibits a fully mesenchymal state on the spectrum of the EMT states.

Mesenchymal clones possess larger cell aspect ratios and lower motile potential

For the purposes of monitoring proliferation, cellular features, and migration propensity *in vitro*, we employed live cell imaging of the parental cells and SCCs utilising phase-focus livecyte imaging (Supplementary Videos). Consistent with the observed morphologies, all mesenchymal clones exhibited substantially lower cellular sphericities ($p < 0.0001$) (Fig. 4A, B) and larger cell aspect ratios ($p < 0.0001$) as compared to the parental line, due primarily to elongated length:width ratios (Fig. 4B and C). Fig. 4B depicts the wide size variation between two clonal cells of HBEC-3KT. Interestingly, analyses of their motility parameters via evaluation of track speed, showed that the mesenchymal clones displayed lower migratory abilities as compared to the HBEC-3KT cells ($p < 0.0001$) (Fig. 4D; Supplementary Video).

Despite the apparent morphological characteristics and canonical EMT marker changes in clones reflecting their enrichment in mesenchymal nature, the SCCs displayed modest to no significant differences in their doubling times, except for mesenchymal-like clone SCC16, which displays an extended doubling time ~2-fold higher then parental cells. The cell doubling time of the parental cell line is 21±5.8 h and for all the SCCs, ranged from 17.2 ± 3 h for SCC8 to 48±8.7 h for SCC16 (Fig. 4E). Collectively, compared to the parental-like clones, mesenchymal clones exhibited statistically significantly lower cellular sphericity ($p < 0.0001$) (Fig. 4F), higher cell aspect ratio ($p < 0.01$) (Fig. 4G) and lower track speed ($p < 0.001$) (Fig. 4H), while doubling times were similar ($p = 0.35$) (Fig. 4I). The lower random cell motility of the mesenchymal clones might imply dysregulation of actin stress fibres or other motility structures. However, the specific mechanism(s) of how the focal adhesions and/or actin stress fibres implement an elongated morphology in the mesenchymal clones (as observed in Figs. 1B, 3A, 4B) but with subverted migratory potential is intriguing, and remains to be fully understood.

Divergent stemness potential across the single cell-derived clones

Concomitant high and low expression of the cell surface adhesion receptor CD44 and the surface antigen CD24 respectively, is also referred to as the $CD44^{high}/CD24^{low}$ state. This state is a well-recognised marker of cancer stemness amongst breast, lung and other cancers [56, 57] and is also associated with a putative EMT phenotype [58]. To test whether the mesenchymal clones have shifted stemness traits, we used FACS analyses to simultaneously assess the expression of the CD44 and CD24 surface markers for the HBEC-3KT cells and our SCCs. Specifically, we determined the proportions of $CD44^{high/low}/CD24^{low/int/hi}$ cellular subpopulations across the HBEC-3KT cells and the derived clones with respect to the known reference $CD44^{high}/CD24^{high}$ state of the MDA-MB-468 breast cancer cell line as a control [59] (82.6% of cells gated in $CD44^{high}/CD24^{high}$ state) (Fig. 5A and B). Surprisingly, HBEC-3KT cells were remarkably stem-like in relation to these markers, as over 75% of all gated cells were within the $CD44^{high}/CD24^{int}$ subpopulation in both the parental cells and five out of the eight clones, including parental-like clones SCC12, SCC14 and SCC20, and mesenchymal clones SCC17 and SCC18. Profoundly, the three remaining clones, parental-like SCC8 and mesenchymal SCC16 and SCC19, displayed a significantly higher proportion of cells in the $CD44^{low}/CD24^{low}$ state with 40–50% of the gated cells residing in that quadrant (Fig. 5A and B). Thus, this represents diversity amongst the clones derived from the HBEC-3KT parental cells in their gated CD44 CD24 subpopulations profiles irrespective of their parental-like and mesenchymal phenotypes. This diversity is further reflected by our observation that we found no statistically significant increase of stemness traits with regards to CD44 and CD24 surface expression between our classified groups (Fig. 5C). Thus, we find no evidence for increased stemness features specific for either the parental-like or the mesenchymal groups.

Diverse morphology behaviour of HBEC-3KT and clones in 3D organotypic culture

We seeded HBEC-3KT cells and the clones in Matrigel™ and assessed their morphological characteristics on days 4 and 8. Interestingly, the morphologies of HBEC-3KT cells and clones were very diverse. HBEC-3KT cells embedded as self-aggregated cells by Day 4 and formed 3D spheroids showing similar cyst-like morphologies by Day 8, as observed previously when cocultured in Matrigel™ below foetal lung fibroblasts [60]. Interestingly, however, all parental-like clones show diversified morphologies when grown within extra-cellular matrix (ECM), except SCC12, whose growth pattern in 3D is similar to that of parental cells. SCC8 and SCC14 cells show elongated spindle protrusions, like mesenchymal clones but less extensive in length. For all mesenchymal clones,

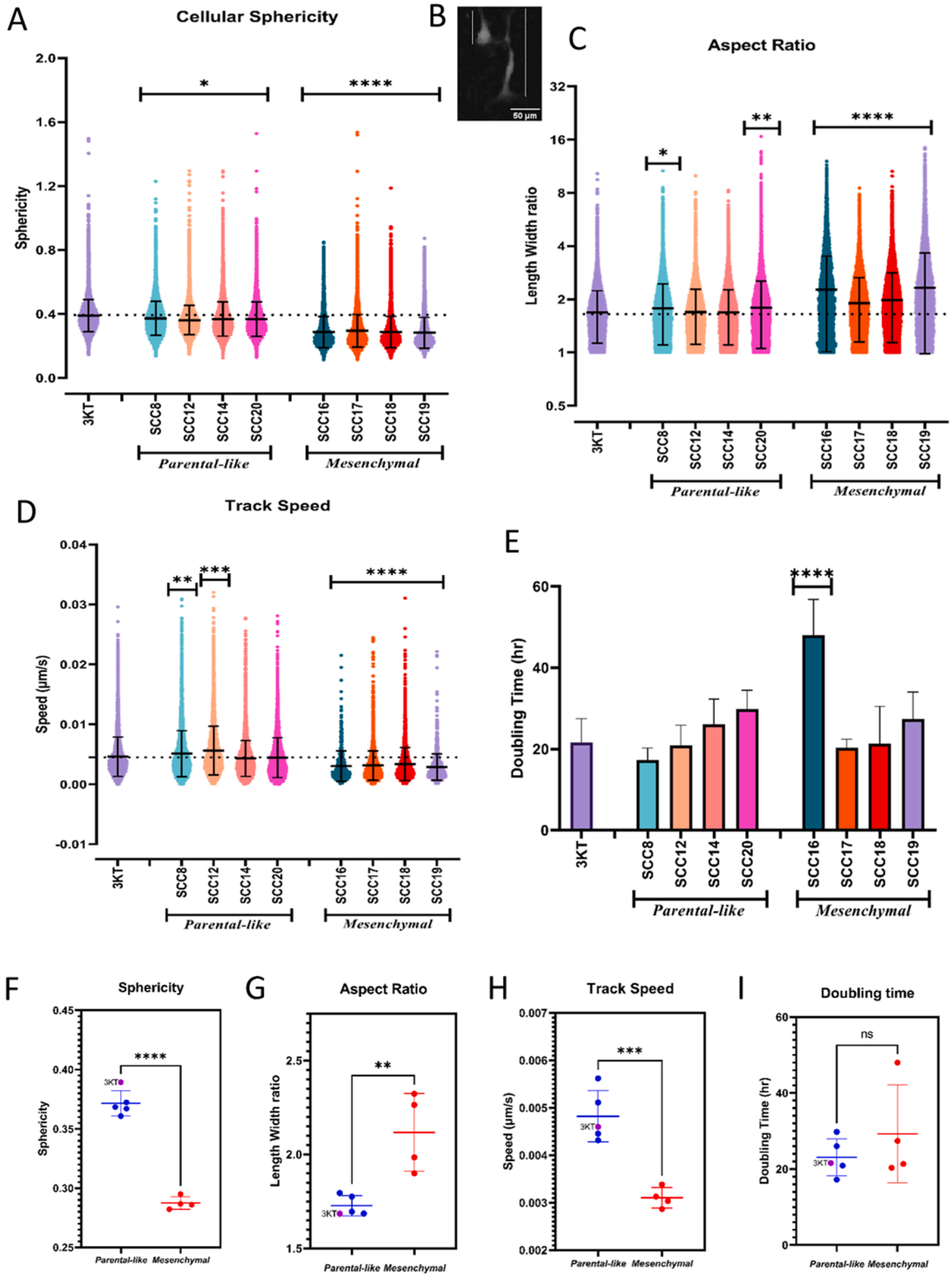

Fig. 4. Cellular functional attribute variations amongst single cell-derived clones and parental HBEC-3KT cells. (A) Interpolation from Livecyte label-free Quantitative Phase Imaging (QPI) data for cellular sphericity. (B) Brightfield image of two cells reflecting wide variation in the aspect ratio from the clones derived from HBEC-3KT cells. (C-E) Interpolation of QPI data, similar to panel (A) but for (C) cell aspect ratios, (D) track speeds and (E) doubling times of the clones and HBEC3-KT parental cells to identify distinct cellular features within heterogeneous cultures. (F-I) Scatter dot plots were plotted for assessing differences between the two groups; parental-like and mesenchymal clones for (F) cellular sphericity (G) cell aspect ratio (H) track speed and (I) doubling time. Statistical tests employed were one-way ANOVA and nonparametric Dunnett's multiple comparisons test for comparing the clones with the parental cells (A, C, D, E) and unpaired *t*-test for comparing two classified groups, parental-like and mesenchymal, for different clonal populations (F, G, H and I). ns: not significant, * $P < 0.05$, ** $P < 0.01$, *** $P < 0.001$, **** $P < 0.0001$.

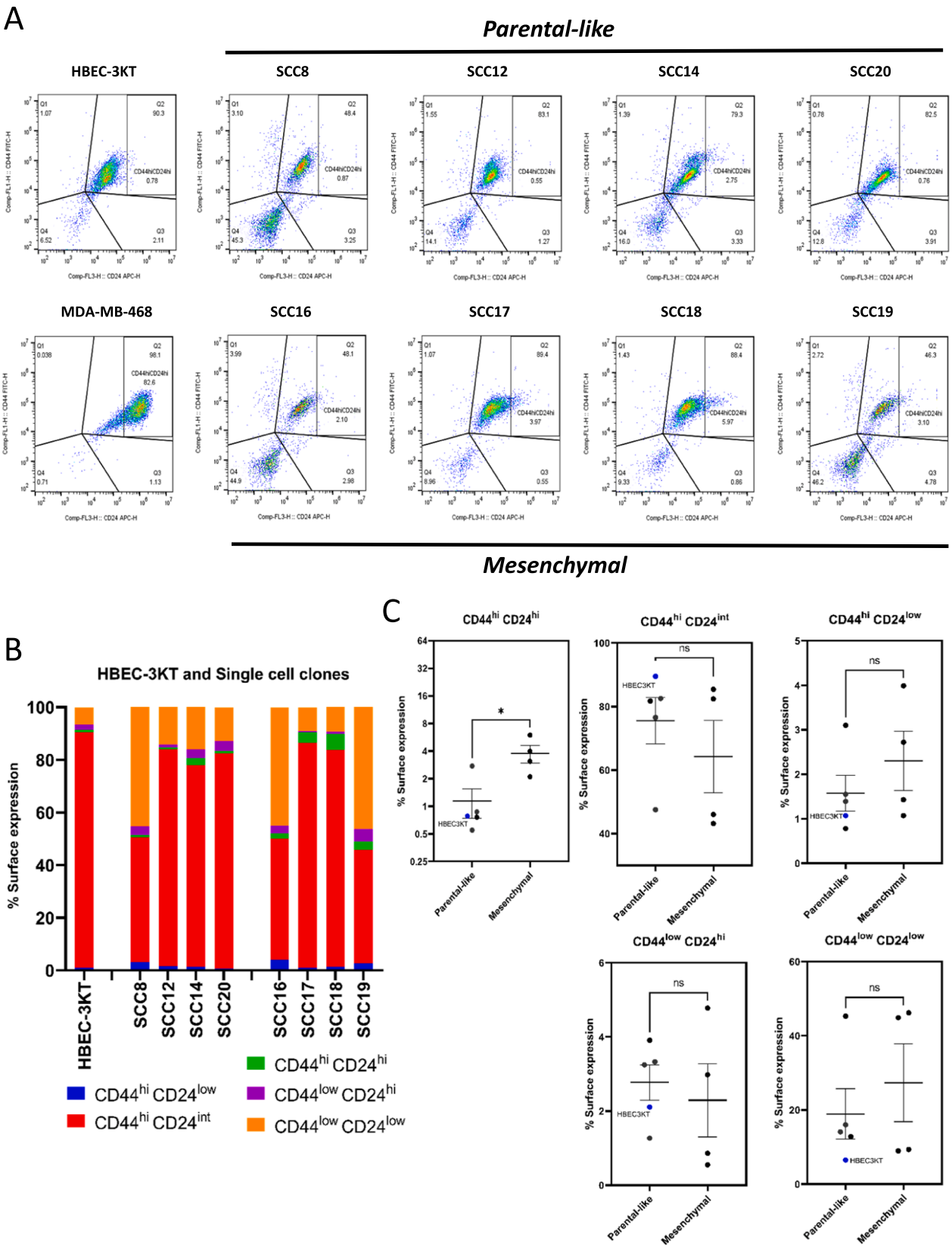

Fig. 5. Assessment of CD44 and CD24 markers for stemness using flow cytometry. (A) The dot plots represent the expression pattern of CD44 (y-axis) and CD24 (x-axis) in the HBEC-3KT cells and the clones. Top panels represent the parental-like clones and the bottom panels represent mesenchymal clones. Gating for different quadrants was plotted with respect to the control breast cancer cell line MDA-MB-468 as a reference (bottom left plot), which is over-represented of $CD44^{hi}CD24^{hi}$ state. (B) Proportions of the subpopulations defined by the combination of the stem cell markers CD44 and CD24 (high, intermediate or low states) in HBEC-3KT cells and the single-cell derived clones (C). Scatter dot plots were plotted for the defined CD44 CD24 subpopulations for assessing differences between the classified two groups, parental-like and mesenchymal for different clonal populations. Statistical analyses were performed using unpaired *t*-test. ns: not significant, * $P < 0.05$.

the cells were very elongated and showed spindle-like protrusions within Matrigel™. Budding of the cells was also observed within ECM as shown for SCC16 on Day 8 (Fig. 6). SCC20 also showed a varied response to cell growth in 3D as cells appear to grow as rounded up along with few spindle-like cell patterns. Together, these results show that in 3D culture, all mesenchymal clones continue to grow with typical mesenchymal spindle-like protrusions, while parental-like clones grow either as round spheroids or as spindly, mesenchymal-like morphologies, albeit that the protrusions of the latter are shorter than those of the mesenchymal clones.

Divergent glycolytic and mitochondrial bioenergetics of HBEC-3KT and clones

Rewiring of the metabolic network is pivotal to meeting cellular energy and biosynthetic demands during tumour growth, metastasis and clonal seeding. We used the Seahorse Extracellular Flux analyser to determine the real-time flux of energy production in HBEC-3KT parental cells and the eight clones through mitochondrial respiration – termed the Oxygen Consumption Rate (OCR) and through glycolytic capacity via lactate excretion – termed the ExtraCellular Acidification Rate (ECAR) [61]. The foremost striking observation in HBEC-3KT and all single-cell generated clones was that glycolysis was the major contributing pathway for ATP and energy production, with a lower contribution through mitochondrial respiration (Fig. 7A). Remarkably, all clones showed statistically significantly altered basal ATP production rates compared to the parental HBEC-3KT cells, although the ATP production rates were highest in two of the mesenchymal clones (SCC17, SCC18) as compared to parental cells, parental-like clones and the other mesenchymal clones (Fig. 7A). Disparity in the energy flux distribution, as measured through ATP rate index – *i.e.*, the $\log_2$ ratio of glycolytic ATP production to mitochondrial ATP production – was apparent, as the rate amongst all the parental-like and mesenchymal clones differed from that of parental HBEC-3KT cells, except for clone SCC14 (Fig. 7B). Also, the rate of glycolytic reserves utilised for energy demand was higher for 5 of the clones (all except SCC14, SCC16 and SCC19) as compared to the parental population, which reflects those clones that have executed metabolic reprogramming in their energy demand to consume for their clonal growth, adaptation, and propagation (Fig. 7B). Though the distribution of ATP production rates (Fig. 7C) and ATP rate indexes (Fig. 7D) varied considerably amongst the parental-like and mesenchymal clones, these differences between the parental-like and mesenchymal clones were not statistically significant. Thus, although the clones showed divergent levels of metabolic rewiring, their bioenergetics did not consistently shift directions between parental-like and mesenchymal clones.

Integrative assessment of functional attributes

We next determined how closely the phenotypic characteristics of the HBEC-3KT single-cell derived clones correlated using integrative analyses of the functional attributes that we analysed. Pearson correlation matrixes (Fig. 8A) reflect associations amongst the eleven functional parameters assessed for the HBEC-3KT parental cells and clones, including doubling time, ATP production rate, cell aspect ratio, track speed, gene expression (ΔCT) for the epithelial and mesenchymal markers EpCAM, CK-19, ZEB1, MMP-2, NCAD, and median fluorescence intensity (MFI) for EpCAM and vimentin. None of the analysed phenotypic parameters statistically significantly correlated with doubling time, ATP production rate or vimentin MFI, whereas significant

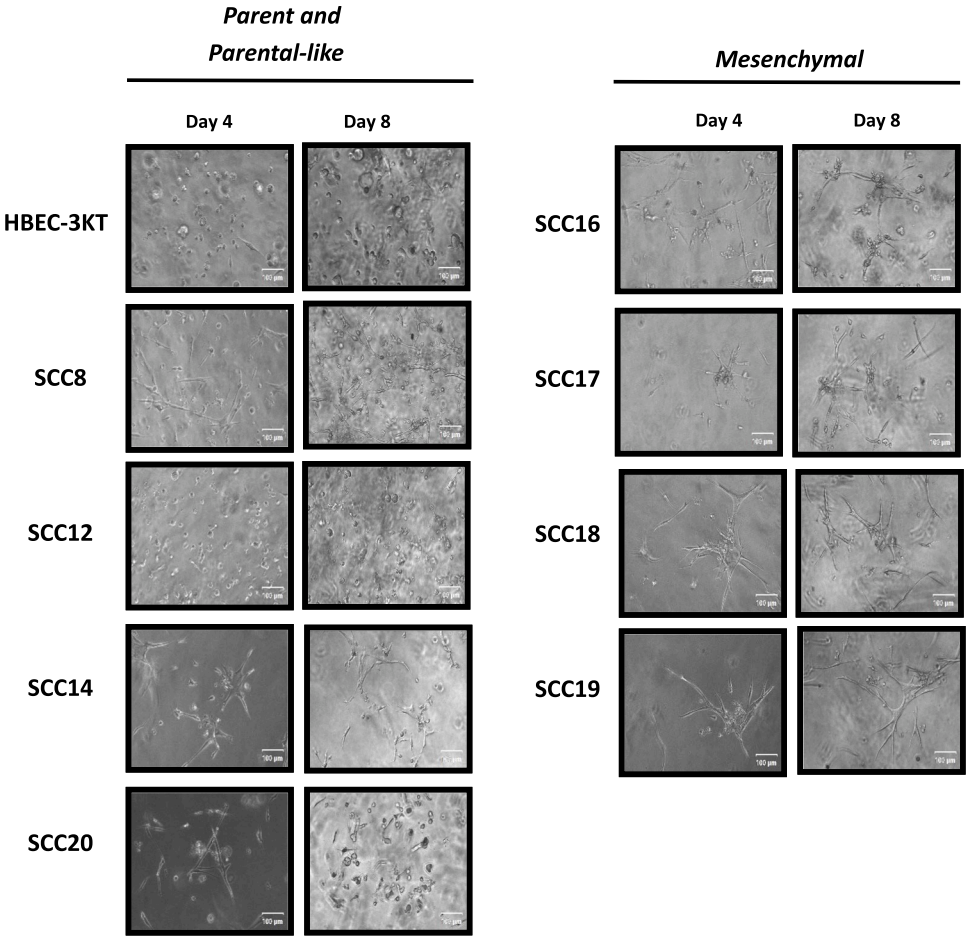

Fig. 6. Seeding of HBEC-3KT and single cell-derived clones within Matrigel™. Culture of the HBEC3-KT cells and single cell derived clones atop of an ECM matrix for 8 days results in diversified culture and morphology behaviour where mesenchymal clones (right panel) show spindle like protrusion. Parental cells and SCC12 (left panel) show cyst-like structure and SCC8, SCC14 and SCC20 (on left panel) embark elongated protrusions although shorter than those of mesenchymal clones on the right panel.
.

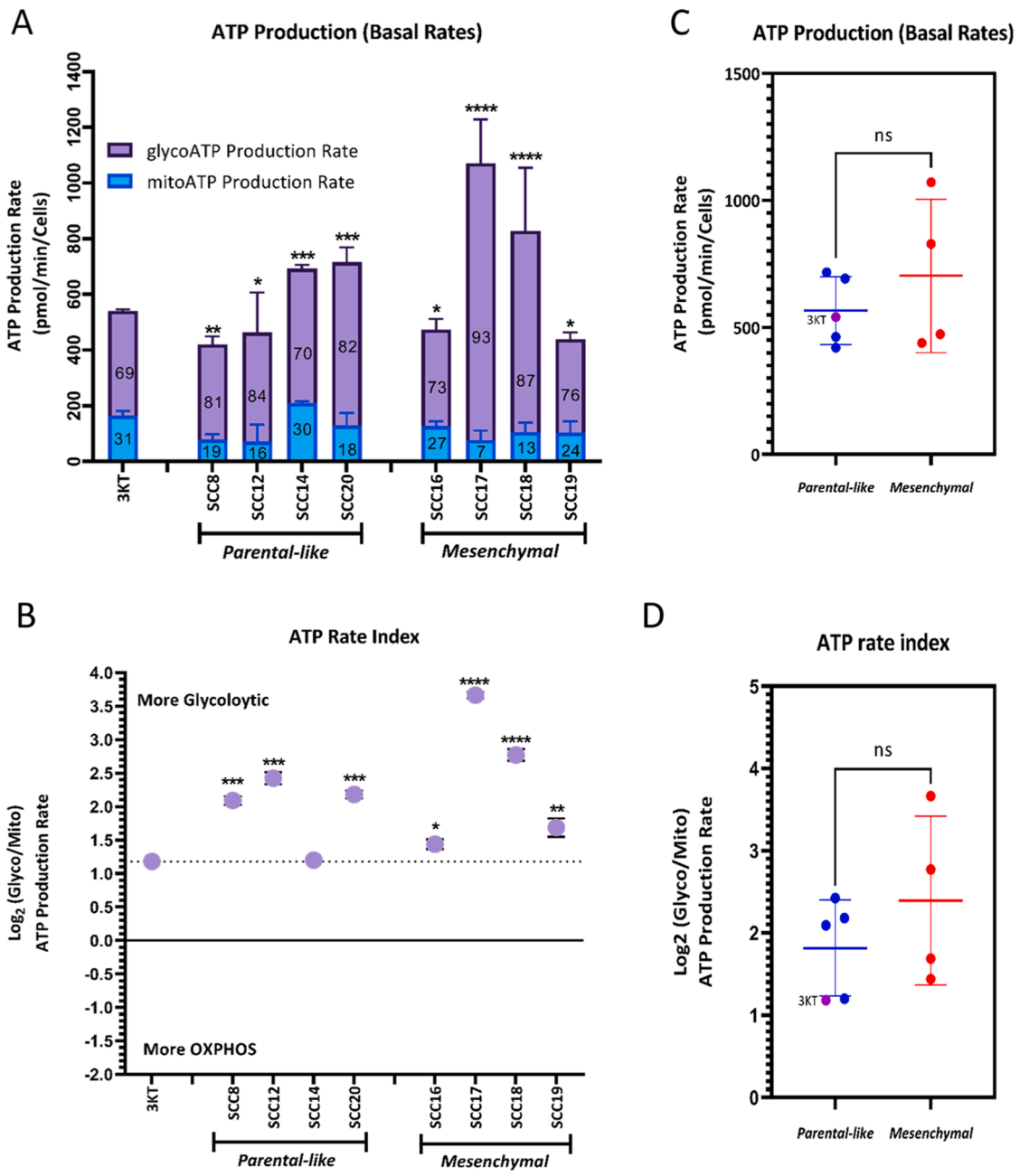

Fig. 7. Mitochondrial profiles of HBEC-3KT and single cell-derived clones. (A) Metabolic flux showing total quantification and percentage (depicted within bars) of ATP production contributed from mitochondria and glycolysis for the HBEC-3KT and single cell-derived clones. (B) The glycoATP/mitoATP ratio of the data in (**A**) was log2-transformed to provide an index of each clone and HBEC-3KT cells for their comparative utilization of glycolytic and oxidative metabolism. (C) Scatter dot plot for the ATP production (basal rate) for assessing the statistical differences between the classified two groups, parental-like and mesenchymal, for different clonal populations. (D) Scatter dot plot for the ATP rate index for assessing the significant differences between the classified two groups, parental-like and mesenchymal, for different clonal populations. Statistical tests employed were one-way ANOVA and nonparametric Dunnett's multiple comparisons test for comparing the clones with the parental cells (A, C) and unpaired *t*-test for comparing two classified groups, parental-like and mesenchymal for different clonal populations (B, D). ns: not significant, * $P < 0.05$, ** $P < 0.01$, *** $P < 0.001$, **** $P < 0.0001$.

correlations were observed between EpCAM MFI and all the remaining phenotypic traits (Supplementary Table S3, S4). EpCAM MFI showed significant positive correlation with ΔCT EPCAM ($R^2 = 0.9308$, $p = 0.00026$), ΔCT CK-19 ($R^2 = 0.8921$, $p = 0.0012$) and track speed ($R^2 = 0.8921$, $p = 0.0070$), and significant negative correlation with ΔCT ZEB1 ($R^2 = -0.925$, $p = 0.00035$), ΔCT MMP-2 ($R^2 = -0.899$, $p = 0.0009$), aspect ratio ($R^2 = -0.861$, $p = 0.0028$) and ΔCT NCAD ($R^2 = -0.811$, $p = 0.0078$). ΔCT NCAD showed significant positive correlation with ΔCT ZEB1 and ΔCT MMP-2. While aspect ratio significantly anti-correlated with track speed ($R^2 = -0.8229$, $p = 0.0064$) and ΔCT CK-19 ($R^2 = -0.8193$, $p = 0.0068$), it correlated positively with ΔCT MMP-2 ($R^2 = 0.8601$, $p = 0.0029$).

To further understand which phenotypic markers or variables were most influential in the PCA patterns, we visualized PC scores (Fig. 8B) and PC loadings (Fig. 8C). These analyses revealed that the mesenchymal clones were again easily segregated from the parental cells and parental-like clones on the PC1 axis with respect to the 11 assessed functional traits (Fig. 8B). Along the PC2 axis wider diversity exists for the mesenchymal clones (range=4, from −2 to 2) compared to the parental-like clones (range=1.7, from −0.8 to 0.9) (Fig. 8B). PC loadings

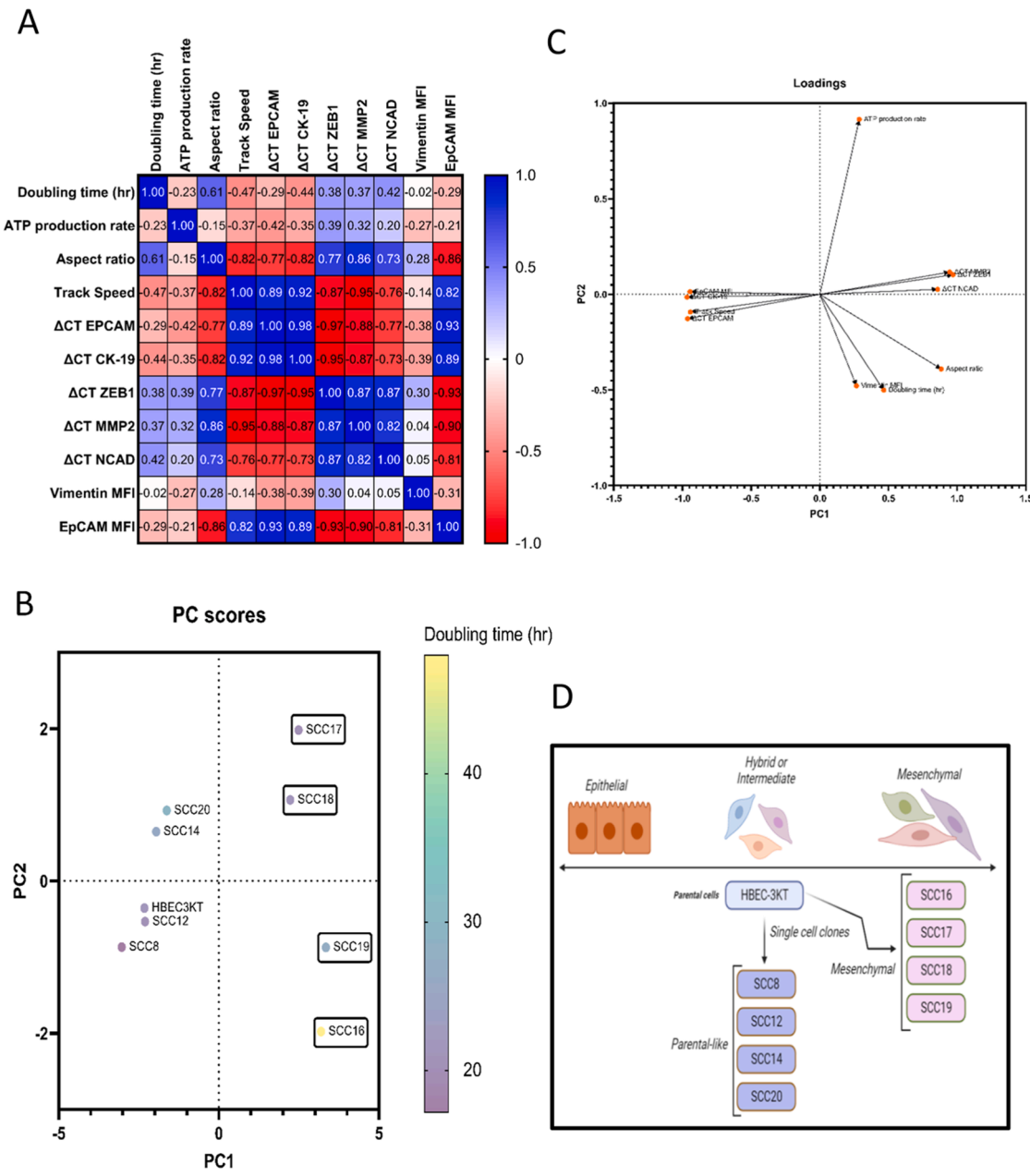

Fig. 8. Integration of the functional and phenotypic analyses of the single cell-derived clones. (A) Pearson correlation matrix for the 11 functional traits assessed *in vitro* (including doubling time, ATP basal rate, aspect ratio, track speed, EpCAM and vimentin protein expression and gene expression of *EpCAM, CK19, Zeb1, MMP-2, N—CAD*. Computed R- and p-values are provided in Supplementary Tables S3 and S4. (B) Principal component (PC) score of HBEC-3KT parent cells and single cell-derived clones assessed based on above mentioned 11 functional parameters. Colour legend is plotted as per the doubling time estimation. Labels with black outline borders represent mesenchymal clones. (C) Loadings plot of the functional parameters from which the PC Score is shown in (B). (D) Schematic illustration of the placement of the parental HBEC-3KT cells and single-cell derived clones on an EMP spectrum between epithelial and mesenchymal states.

(Fig. 8C) showed that PC1 was most positively influenced by gene expression markers for mesenchymal genes including ΔCT ZEB1 (r = 0.97), ΔCT MMP2 (r = 0.94), ΔCT NCAD (r =0.85), and was negatively impacted by epithelial gene expression markers ΔCT EPCAM (r = −0.96), ΔCT CK-19 (r = −0.96) and EpCAM MFI (r = −0.94) and track speed (r = −0.94). PC2 was positively associated with ATP production rate (r = 0.91), and negatively associated with doubling time (r = −0.5), aspect ratio (r = −0.39) and vimentin MFI (r = −0.47). Thus, our integrative analyses of all investigated functional attributes validate that the distinct morphologies of our clones coincide with functional differences. In addition, they unveil the specific contributions of each of the investigated parameters.

Discussion

Although mutations and aneuploidy shape tumour evolution and disease prognosis clinically [62,63], it is altogether both the genetic and non-genetic duality of cancer functional heterogeneity that shape the course of cancer initiation, progression and chemo- and immune-therapy responses. Intratumoral heterogeneity not only encompasses genomic or chromosomal instability but also manifests changes at transcriptional, epigenetic, phenotypic, signalling and metabolic levels [64,65]. Furthermore, clonal selection and evolution is a prominent deterministic factor influenced by both genetic and non-genetic contributions, which jointly drive tumour progression, chemoresistance and metastatic seeding [66]. Thus, generating and

studying cellular models that delineate the functional characteristics of the clonal diversity can herald a major refinement in our understanding of the cellular phenotypic plasticity that imparts intratumoral heterogeneity.

To study this pragmatically, we first generated single cell-derived clones from HBEC-3KT parental cultures by limited dilution and characterised these with respect to various cellular traits, such as EMT marker expression, migratory potential, stemness profiling and real time bioenergetics analysis for ATP basal production rate. The HBEC-3KT-derived clones exhibited dramatic differences with respect to their molecular and functional attributes. Based on their cellular morphology (Fig. 1B), we classified the clones into two groups, parental-like and mesenchymal SSCs, and validated the segregation further using gene and protein expression changes for EMT markers, such as vimentin and EpCAM. Our isolated clones represent stable variants of the extreme mesenchymal state with no dynamicity and reversibility. Although tissue-specific associations between genomic alterations and metastasis have been discovered [63,67], there are indeed only few studies where the concordance of EMT with mutational dependencies, chromosomal instability and/or copy number alterations have been studied across any cancer type on a cellular level, including the HBEC-3KT model studied here [49,68,69]. Importantly, our SNP array profiling indicated that the intrinsic phenotypic plasticity that we observed in the clones from HBEC-3KT parental cells was not influenced by chromosomal aberrations or instability (Supplementary Fig. 1).

Through our RT-qPCR studies, we identified and validated the changes in various EMP-associated canonical markers. PCA clustering also separated mesenchymal SCCs well from parental-like SCCs and parental cells, in particular across PC1, based on the repertoire of EMP and stemness markers studied (Fig. 2C). Mesenchymal grouped clones showed evidence of downregulation of *EpCAM, CK19* and *GRHL2* expression and upregulation of *NCAD, ZEB1, SOX2 and MMP2, ITGB5* although no changes in *VIM* and *FN1* were observed (Fig. 2A and B). Interestingly, the extent of downregulation of epithelial gene expression was extreme compared to the fold-changes in increased gene expression of mesenchymal markers. This suggests that robust loss of epithelial marker genes *per se* contributed to the distinct mesenchymal phenotype within this group of mesenchymal SCCs. Interestingly, we observed upregulation of *TGFBR2* expression and simultaneously downregulation of *BMP-7,* which counter-regulates the TGFβ-Smad signalling amongst many clones, irrespective of their parental-like and mesenchymal grouping as compared to parental cells. Thus, consistent with previous reports [49] and in our context-dependent scenario, this suggests that in HBEC-3KT, TGFβ as cytokine or as a constituent of serum growth factors plays an important role in clonal propagation, evolution and/or maintenance of EMT. Also, our qRT-PCR analysis illustrated *ZEB1* and its target *GRHL2* profound expression differences at the clonal level in the mesenchymal clones. *GRHL2* has been reported as an essential factor in priming epithelial genes whereas Zeb1 can co-opt multiple genomic entities to express and maintain epithelial differentiation in human cells, also verified in the transcriptional landscape studies of derived epithelial and mesenchymal clones from breast immortalized HMLE-Twist1-ER cells [70].

Immunofluorescence analysis of the mesenchymal marker vimentin and the epithelial marker EpCAM, revealed varying levels of expression amongst the clones (Fig. 3). The number of EpCAM-positive cells and EpCAM median intensity were significantly lower in the mesenchymal group as compared to parental cells. The presence of vimentin staining along with EpCAM across parental and parental-like cells represents the hybrid-like EMT phenotype state. Recently, the characterization of subpopulations from breast, lung, pancreatic and skin tumours has indicated that tumour cells with hybrid phenotypes or partial EMT are more capable of dissemination and metastasis then the cells exhibiting an extreme mesenchymal phenotype [14,18,21,34].

The results from our *livecyte* analyses leverage the power of individual cell measurements for evaluating the dynamic cellular features of the parental cells and the individual clones [71]. All mesenchymal spindle-shaped clones display lower sphericity and higher aspect-ratio (Fig. 4), reflecting that this group have enhanced membrane protrusions, which we also observed by vimentin staining (Fig. 3). However, the lower motile ability seen in the mesenchymal SCC group raises the speculation that they might possess a defect in their actin cytoskeleton or actin stress fibre bundles, which facilitate cell movement. We also noted that these mesenchymal clones express low levels of LAMC2 (Fig. 2A), suggesting that the changes in their mesenchymal phenotype might be a result of actin-stress fibre changes. This also suggest the presence of interclonal cooperativity [72] and the heterotypic enhancement that others have seen in mixed populations of epithelial and metaplastic cells in regards to the expression of MMPs and TIMPs [73]. Also, the doubling time (Fig. 4D) did not relate to mesenchymal phenotype, except for SCC16, which was relatively dormant or slowly proliferating, consistent with studies reflecting that EMT induction can result in cell cycle arrest and metabolic quiescence [74]. Since SCC16 was the only clonal population exhibiting this, it may possess some additional factor(s) required for the proliferative loss. Further, the assessment of metabolic ATP production pathways in parental HBEC-3KT cells and subclones revealed highly clone-specific effects (Fig. 7). No clear correlation between phenotype-classified SCCs and metabolic flux changes could be identified in our context-dependent model, but a surge in the glycolytic index for ATP production was observed for several of the clones (Fig. 7B). These changes in the metabolic reprogramming of the SCC does illustrates the relevance of studying metabolic profile in context to clonal characteristics to fully understand the energetic demand, which could ultimately guide therapy treatment [75]. Although we used common markers ($CD44^{hi}/CD24^{low}$) for defining CSC-like cells [76] and to delineate the subpopulations amongst the clones, we did not functionally validate the stemness of these cells. In our SCCs, we observe disparities in their surface marker expression of CD44 and CD24. Nonetheless, the mesenchymal clones show a salient increase in their $CD44^{hi}/CD24^{hi}$ state out of all subpopulations compared to the parental-like group ($p < 0.05$) (Fig. 5). Interestingly, some studies have reported that pEMT (partial or intermediate EMT) characterised through $CD44^{hi}/CD24^{hi}$ state can exhibit stemness-traits [33,77]. This ambiguity suggests that careful interpretation of stemness in regards to the reported CD44 and CD24 markers is required [78].

Although the HBEC-3KT cells that we use are immortalized, they are not cancerous, because their genomes are near-diploid, their p53 pathway function is intact, they show contact-inhibition, have the ability to differentiate, and they fail to grow both *in vitro* under anchorage-independent conditions and *in vivo*, not forming tumours in immunodeficient mice (references [49,52,60,79,80] and our present study). Moreover, the differential growth pattern of the mesenchymal clones within ECM extract as compared to parental HBEC-3KT cells display full characteristics of basal cells from which these cells were derived [60]. This has important implications for our understanding of the development of non-small cell lung cancer (NSCLC), as it suggests that non-cancerous lung epithelial cells may possess EMP prior to transformation of normal lung cells into lung cancer cells. This also suggests that cellular features that promote metastasis may be acquired prior to the acquisition of genomic alterations and tumorigenesis. We observe that changes in cell morphology and gene expression can occur in non-cancerous cells in the absence of genetic alterations. Thus, these changes are epigenetic. Hence, our work has key implications for epigenetic targeted therapies which may be effective in preventing cancer cell morphological changes that are associated with metastasis – either alone or in combination with other therapies.

Altogether, our study emphasises the functional heterogeneity present in the single cell-derived clones. However, the dynamics of clonal heterogeneity and the molecular drivers that induced the phenotypic state transitions remain to be identified. Notably, our study did not identify a mechanism, such as specific signalling pathway, that

underpins the changes observed in the mesenchymal clones. However, it will be interesting to investigate whether induction or modulation of certain pathways, such as cytokines-mediated signalling, including ERK/MAPK and TGFβ-Smad signalling, contributes significantly to the derivation of this phenotypic plasticity. Further, attributes assessed for the differences in drug response and stem-like properties of the clones would be warranted to delineate the full functional heterogeneity of the clones. Epigenetic treatments may prevent tumour formation altogether, as we observe these epigenetic alterations prior to cancerous transformation. Overall, our results provide unprecedented information on the clonal dynamics with regards to EMT, in the absence of genomic heterogeneity, as well as, importantly, in non-cancerous lung cells. The stable clonal phenotypic and functional heterogeneity observed and evaluated in parental-like and extreme mesenchymal-classified SCCs represents the intrinsic plasticity present in HBEC-3KT cells.

Conclusion

Our study provides a significant contribution in describing and understanding the key molecular hallmark properties of isogenic, yet different single-cell clones derived from non-cancerous HBEC-3KT lung epithelial cells. This has improved our understanding of the aetiology of the lung cancer, where non-genetic diversity present within cancer imparts distinct functional characteristics to the cancer. Interrogation of the clones for their attributes including morphology, migration, metabolic profile, stemness genes and markers, and for various transcriptional EMP status garnered functional aspects of the intratumoral heterogeneity influenced in association with or independent of the intrinsic epithelial-mesenchymal plasticity observed amongst the clones.

CRediT authorship contribution statement

Sugandha Bhatia: Conceptualization, Writing – original draft, Methodology, Formal analysis, Data curation, Validation. **Jennifer H Gunter:** Data curation, Formal analysis, Writing – review & editing. **Joshua T Burgess:** Formal analysis, Writing – review & editing. **Mark N Adams:** Resources, Writing – review & editing. **Kenneth O'Byrne:** Resources, Writing – review & editing. **Erik W Thompson:** Supervision, Writing – review & editing. **Pascal HG Duijf:** Conceptualization, Supervision, Funding acquisition, Project administration, Formal analysis, Writing – review & editing.

Declaration of Competing Interest

The authors declare that they have no known competing financial interests or personal relationships that could have appeared to influence the work reported in this paper.

Acknowledgements

This research was funded by the Cancer Council NSW, Project Grant RG 21-13 (to PHGD) and the TRI Foundation, EMCR Cancer Research Grant (to SB). We would like to thank the FACS core facility and Microscopy core facility and Ms. Briony Claxton for Seahorse experiment based at Translational Research Institute (TRI) for their technical assistance. SNP array profiling was done at Australian Translational Genomics Centre (ATGC) which is a partnership between QUT, Pathology QLD and Metro South based at Princess Alexandra Hospital Facility. The Translational Research Institute receives support from the Australian Government.

Supplementary materials

Supplementary material associated with this article can be found, in the online version, at doi:10.1016/j.tranon.2023.101760.

References

[1] J. Ferlay, M. Colombet, I. Soerjomataram, D.M. Parkin, M. Piñeros, A. Znaor, F. Bray, Cancer statistics for the year 2020: an overview, Int. J. Cancer (2021).
[2] Y. Shlyakhtina, K.L. Moran, M.M. Portal, Genetic and non-genetic mechanisms underlying cancer evolution, Cancers (Basel) 13 (6) (2021) 1380.
[3] P.H.G. Duijf, D. Nanayakkara, K. Nones, S. Srihari, M. Kalimutho, K.K. Khanna, Mechanisms of genomic instability in breast cancer, Trend. Mol. Med. 25 (7) (2019) 595–611.
[4] D. Hanahan, Hallmarks of cancer: new dimensions, Cancer Discov. 12 (1) (2022) 31–46.
[5] A. Sharma, E. Merritt, X. Hu, A. Cruz, C. Jiang, H. Sarkodie, Z. Zhou, J. Malhotra, G.M. Riedlinger, S. De, Non-genetic intra-tumor heterogeneity is a major predictor of phenotypic heterogeneity and ongoing evolutionary dynamics in lung tumors, Cell Rep. 29 (8) (2019) 2164–2174, e5.
[6] I. Dagogo-Jack, A.T. Shaw, Tumour heterogeneity and resistance to cancer therapies, Nat. Rev. Clin. Oncol. 15 (2) (2018) 81–94.
[7] Q. Guo, M. Spasic, A.G. Maynard, G.J. Goreczny, A. Bizuayehu, J.F. Olive, P. van Galen, S.S. McAllister, Clonal barcoding with qPCR detection enables live cell functional analyses for cancer research, Nat. Commun. 13 (1) (2022) 3837.
[8] M. Janiszewska, D.P. Tabassum, Z. Castaño, S. Cristea, K.N. Yamamoto, N. L. Kingston, K.C. Murphy, S. Shu, N.W. Harper, C.G. Del Alcazar, Subclonal cooperation drives metastasis by modulating local and systemic immune microenvironments, Nat. Cell Biol. 21 (7) (2019) 879–888.
[9] N.R. Campbell, A. Rao, M.V. Hunter, M.K. Sznurkowska, L. Briker, M. Zhang, M. Baron, S. Heilmann, M. Deforet, C. Kenny, L.P. Ferretti, T.-H. Huang, S. Perlee, M. Garg, J. Nsengimana, M. Saini, E. Montal, M. Tagore, J. Newton-Bishop, M. R. Middleton, P. Corrie, D.J. Adams, R. Rabbie, N. Aceto, M.P. Levesque, R. A. Cornell, I. Yanai, J.B. Xavier, R.M. White, Cooperation between melanoma cell states promotes metastasis through heterotypic cluster formation, Dev. Cell 56 (20) (2021) 2808–2825, e10.
[10] T. Brabletz, R. Kalluri, M.A. Nieto, R.A. Weinberg, EMT in cancer, Nat. Rev. Cancer 18 (2) (2018) 128–134.
[11] E.D. Williams, D. Gao, A. Redfern, E.W. Thompson, Controversies around epithelial–mesenchymal plasticity in cancer metastasis, Nat. Rev. Cancer 19 (12) (2019) 716–732.
[12] J. Yang, P. Antin, G. Berx, C. Blanpain, T. Brabletz, M. Bronner, K. Campbell, A. Cano, J. Casanova, G. Christofori, S. Dedhar, R. Derynck, H.L. Ford, J. Fuxe, A. García de Herreros, G.J. Goodall, A.-K. Hadjantonakis, R.J.Y. Huang, C. Kalcheim, R. Kalluri, Y. Kang, Y. Khew-Goodall, H. Levine, J. Liu, G. D. Longmore, S.A. Mani, J. Massagué, R. Mayor, D. McClay, K.E. Mostov, D. F. Newgreen, M.A. Nieto, A. Puisieux, R. Runyan, P. Savagner, B. Stanger, M. P. Stemmler, Y. Takahashi, M. Takeichi, E. Theveneau, J.P. Thiery, E. W. Thompson, R.A. Weinberg, E.D. Williams, J. Xing, B.P. Zhou, G. Sheng, E.M.T.I. A. On behalf of the, Guidelines and definitions for research on epithelial–mesenchymal transition, Nat. Rev. Molecul. Cell Biol. 21 (6) (2020) 341–352.
[13] M.P. Mak, P. Tong, L. Diao, R.J. Cardnell, D.L. Gibbons, W.N. William, F. Skoulidis, E.R. Parra, J. Rodriguez-Canales, I.I. Wistuba, A patient-derived, pan-cancer EMT signature identifies global molecular alterations and immune target enrichment following epithelial-to-mesenchymal TransitionPan-cancer EMT molecular and immune alterations, Clin. Cancer Res. 22 (3) (2016) 609–620.
[14] I. Pastushenko, A. Brisebarre, A. Sifrim, M. Fioramonti, T. Revenco, S. Boumahdi, A. Van Keymeulen, D. Brown, V. Moers, S. Lemaire, Identification of the tumour transition states occurring during EMT, Nature 556 (7702) (2018) 463–468.
[15] A.P. Patel, I. Tirosh, J.J. Trombetta, A.K. Shalek, S.M. Gillespie, H. Wakimoto, D. P. Cahill, B.V. Nahed, W.T. Curry, R.L. Martuza, Single-cell RNA-seq highlights intratumoral heterogeneity in primary glioblastoma, Science 344 (6190) (2014) 1396–1401.
[16] S.V. Puram, I. Tirosh, A.S. Parikh, A.P. Patel, K. Yizhak, S. Gillespie, C. Rodman, C. L. Luo, E.A. Mroz, K.S. Emerick, Single-cell transcriptomic analysis of primary and metastatic tumor ecosystems in head and neck cancer, Cell 171 (7) (2017) 1611–1624, e24.
[17] M.S. Brown, B. Abdollahi, O.M. Wilkins, H. Lu, P. Chakraborty, N.B. Ognjenovic, K. E. Muller, M.K. Jolly, B.C. Christensen, S. Hassanpour, D.R. Pattabiraman, Phenotypic heterogeneity driven by plasticity of the intermediate EMT state governs disease progression and metastasis in breast cancer, Sci. Adv. 8 (31) (2022) eabj8002.
[18] K.P. Simeonov, C.N. Byrns, M.L. Clark, R.J. Norgard, B. Martin, B.Z. Stanger, J. Shendure, A. McKenna, C.J. Lengner, Single-cell lineage tracing of metastatic cancer reveals selection of hybrid EMT states, Cancer Cell 39 (8) (2021) 1150–1162, e9.
[19] M.K. Jolly, M. Boareto, B. Huang, D. Jia, M. Lu, E. Ben-Jacob, J.N. Onuchic, H. Levine, Implications of the hybrid epithelial/mesenchymal phenotype in metastasis, Front. Oncol. 5 (2015) 155.
[20] M.K. Jolly, S.A. Mani, H. Levine, Hybrid epithelial/mesenchymal phenotype(s): the 'fittest' for metastasis? Biochimica et Biophysica Acta (BBA) - Reviews on Cancer 1870 (2) (2018) 151–157.
[21] M.K. Jolly, R.J. Murphy, S. Bhatia, H.J. Whitfield, A. Redfern, M.J. Davis, E. W. Thompson, Measuring and modelling the epithelial- mesenchymal hybrid state in cancer: clinical implications, Cell. Tissue. Organ. (Print) 211 (2) (2022) 110–133.
[22] S. Bhatia, P. Wang, A. Toh, E.W. Thompson, New insights into the role of phenotypic plasticity and EMT in driving cancer progression, Front Mol. Biosci. 7 (71) (2020).

[23] S. Bhatia, J. Monkman, A.K.L. Toh, S.H. Nagaraj, E.W. Thompson, Targeting epithelial-mesenchymal plasticity in cancer: clinical and preclinical advances in therapy and monitoring, Biochem. J. 474 (19) (2017) 3269–3306.

[24] S. Bhatia, T. Blick, C. Pinto, M. Waltham, J. Monkman, E. Ivanova, P.M. Pollock, S. H. Nagaraj, A.P. Wiegmans, I. Haviv, K.J. Simpson, E.W. Thompson, Identifying therapies to combat epithelial mesenchymal plasticity-associated chemoresistance to conventional breast cancer therapies using an shRNA library screen, Cancers (Basel) 12 (5) (2020) 1123.

[25] A. Dongre, M. Rashidian, F. Reinhardt, A. Bagnato, Z. Keckesova, H.L. Ploegh, R. A. Weinberg, Epithelial-to-mesenchymal transition contributes to immunosuppression in breast carcinomas, Cancer Res. 77 (15) (2017) 3982–3989.

[26] S. Kim, J. Koh, M.Y. Kim, D. Kwon, H. Go, Y.A. Kim, Y.K. Jeon, D.H. Chung, PD-L1 expression is associated with epithelial-to-mesenchymal transition in adenocarcinoma of the lung, Hum. Pathol. 58 (2016) 7–14.

[27] L. Chen, D.L. Gibbons, S. Goswami, M.A. Cortez, Y.-H. Ahn, L.A. Byers, X. Zhang, X. Yi, D. Dwyer, W. Lin, L. Diao, J. Wang, J.D. Roybal, M. Patel, C. Ungewiss, D. Peng, S. Antonia, M. Mediavilla-Varela, G. Robertson, S. Jones, M. Suraokar, J. W. Welsh, B. Erez, I.I. Wistuba, L. Chen, D. Peng, S. Wang, S.E. Ullrich, J. V. Heymach, J.M. Kurie, F.X.-F. Qin, Metastasis is regulated via microRNA-200/ZEB1 axis control of tumour cell PD-L1 expression and intratumoral immunosuppression, Nat. Commun. 5 (1) (2014) 5241.

[28] A. Dongre, M. Rashidian, E.N. Eaton, F. Reinhardt, P. Thiru, M. Zagorulya, S. Nepal, T. Banaz, A. Martner, S. Spranger, R.A. Weinberg, Direct and indirect regulators of epithelial-mesenchymal transition-mediated immunosuppression in breast carcinomas, Cancer Discov. 11 (5) (2021) 1286–1305.

[29] S. Sahoo, S.P. Nayak, K. Hari, P. Purkait, S. Mandal, A. Kishore, H. Levine, M. K. Jolly, Immunosuppressive traits of the hybrid epithelial/mesenchymal phenotype, Front. Immunol. 12 (2021), 797261.

[30] V.L. Chin, C.L. Lim, Epithelial-mesenchymal plasticity-engaging stemness in an interplay of phenotypes, Stem Cell Investig. 6 (2019) 25.

[31] P. Balcik-Ercin, L. Cayrefourcq, R. Soundararajan, S.A. Mani, C. Alix-Panabières, Epithelial-to-mesenchymal plasticity in circulating tumor cell lines sequentially derived from a patient with colorectal cancer, Cancers (Basel) 13 (21) (2021).

[32] S. Hassan, T. Blick, E.W. Thompson, E.D. Williams, Diversity of epithelial-mesenchymal phenotypes in circulating tumour cells from prostate cancer patient-derived xenograft models, Cancers (Basel) 13 (11) (2021).

[33] A. Grosse-Wilde, A. Fouquier d'Hérouël, E. McIntosh, G. Ertaylan, A. Skupin, R. E. Kuestner, A. del Sol, K.-A. Walters, S. Huang, Stemness of the hybrid epithelial/mesenchymal state in breast cancer and its association with poor survival, PLoS One 10 (5) (2015), e0126522.

[34] I. Pastushenko, F. Mauri, Y. Song, F. de Cock, B. Meeusen, B. Swedlund, F. Impens, D. Van Haver, M. Opitz, M. Thery, Y. Bareche, G. Lapouge, M. Vermeersch, Y.-R. Van Eycke, C. Balsat, C. Decaestecker, Y. Sokolow, S. Hassid, A. Perez-Bustillo, B. Agreda-Moreno, L. Rios-Buceta, P. Jaen, P. Redondo, R. Sieira-Gil, J.F. Millan-Cayetano, O. Sanmatrtin, N. D'Haene, V. Moers, M. Rozzi, J. Blondeau, S. Lemaire, S. Scozzaro, V. Janssens, M. De Troya, C. Dubois, D. Pérez-Morga, I. Salmon, C. Sotiriou, F. Helmbacher, C. Blanpain, Fat1 deletion promotes hybrid EMT state, tumour stemness and metastasis, Nature 589 (7842) (2021) 448–455.

[35] M.K. Jolly, J.A. Somarelli, M. Sheth, A. Biddle, S.C. Tripathi, A.J. Armstrong, S. M. Hanash, S.A. Bapat, A. Rangarajan, H. Levine, Hybrid epithelial/mesenchymal phenotypes promote metastasis and therapy resistance across carcinomas, Pharmacol. Ther. 194 (2019) 161–184.

[36] B. Kvokačková, J. Remšík, M.K. Jolly, K. Souček, Phenotypic heterogeneity of triple-negative breast cancer mediated by epithelial-mesenchymal plasticity, Cancers (Basel) 13 (9) (2021).

[37] C. Kroger, A. Afeyan, J. Mraz, E.N. Eaton, F. Reinhardt, Y.L. Khodor, P. Thiru, B. Bierie, X. Ye, C.B. Burge, R.A. Weinberg, Acquisition of a hybrid E/M state is essential for tumorigenicity of basal breast cancer cells, Proc. Natl. Acad. Sci. U.S. A. 116 (15) (2019) 7353–7362.

[38] K. Vipparthi, K. Hari, P. Chakraborty, S. Ghosh, A.K. Patel, A. Ghosh, N.K. Biswas, R. Sharan, P. Arun, M.K. Jolly, S. Singh, Emergence of hybrid states of stem-like cancer cells correlates with poor prognosis in oral cancer, iScience 25 (5) (2022), 104317.

[39] S. Sahoo, B. Ashraf, A.S. Duddu, A. Biddle, M.K. Jolly, Interconnected high-dimensional landscapes of epithelial-mesenchymal plasticity and stemness in cancer, Clin. Exp. Metastasis 39 (2) (2022) 279–290.

[40] F. Lüönd, N. Sugiyama, R. Bill, L. Bornes, C. Hager, F. Tang, N. Santacroce, C. Beisel, R. Ivanek, T. Bürglin, S. Tiede, J. van Rheenen, G. Christofori, Distinct contributions of partial and full EMT to breast cancer malignancy, Dev. Cell 56 (23) (2021) 3203–3221, e11.

[41] M. Tong, Z. Deng, M. Yang, C. Xu, X. Zhang, Q. Zhang, Y. Liao, X. Deng, D. Lv, X. Zhang, Transcriptomic but not genomic variability confers phenotype of breast cancer stem cells, Cancer Commun. 38 (1) (2018) 1–16.

[42] C.L. Chaffer, I. Brueckmann, C. Scheel, A.J. Kaestli, P.A. Wiggins, L.O. Rodrigues, M. Brooks, F. Reinhardt, Y. Su, K. Polyak, Normal and neoplastic nonstem cells can spontaneously convert to a stem-like state, Proceed. Natl. Acad. Sci. 108 (19) (2011) 7950–7955.

[43] R.A. Mathis, E.S. Sokol, P.B. Gupta, Cancer cells exhibit clonal diversity in phenotypic plasticity, Open Biol. 7 (2) (2017).

[44] S. Bhatia, J. Monkman, T. Blick, C. Pinto, M. Waltham, S.H. Nagaraj, E.W. Thompson, Interrogation of Phenotypic Plasticity between Epithelial and Mesenchymal States in Breast Cancer, 8(6) (2019) 893.

[45] H. Ungefroren, I. Thürling, B. Färber, T. Kowalke, T. Fischer, L.V.M. De Assis, R. Braun, D. Castven, H. Oster, B. Konukiewitz, U.F. Wellner, H. Lehnert, J. U. Marquardt, The quasimesenchymal pancreatic ductal epithelial cell line PANC-1-A useful model to study clonal heterogeneity and EMT subtype shifting, Cancers (Basel) 14 (9) (2022).

[46] C. Kim, R. Gao, E. Sei, R. Brandt, J. Hartman, T. Hatschek, N. Crosetto, T. Foukakis, N.E. Navin, Chemoresistance evolution in triple-negative breast cancer delineated by single-cell sequencing, Cell 173 (4) (2018) 879–893, e13.

[47] D. Hanahan, R.A. Weinberg, Hallmarks of cancer: the next generation, Cell 144 (5) (2011) 646–674.

[48] M.V. Liberti, J.W. Locasale, The Warburg effect: how does it benefit cancer cells? Trend. Biochem. Sci. 41 (3) (2016) 211–218.

[49] M. Sato, J.E. Larsen, W. Lee, H. Sun, D.S. Shames, M.P. Dalvi, R.D. Ramirez, H. Tang, J.M. DiMaio, B. Gao, Y. Xie, I.I. Wistuba, A.F. Gazdar, J.W. Shay, J. D. Minna, Human lung epithelial cells progressed to malignancy through specific oncogenic manipulations, Mol. Cancer Res. 11 (6) (2013) 638–650.

[50] J.E. Larsen, V. Nathan, J.K. Osborne, R.K. Farrow, D. Deb, J.P. Sullivan, P. D. Dospoy, A. Augustyn, S.K. Hight, M. Sato, L. Girard, C. Behrens, I.I. Wistuba, A. F. Gazdar, N.K. Hayward, J.D. Minna, ZEB1 drives epithelial-to-mesenchymal transition in lung cancer, J. Clin. Invest. 126 (9) (2016) 3219–3235.

[51] M.L. New, C.M. White, P. McGonigle, D.G. McArthur, L.D. Dwyer-Nield, D. T. Merrick, R.L. Keith, M.A. Tennis, Prostacyclin and EMT pathway markers for monitoring response to lung cancer chemoprevention, Cancer Prevent. Res. 11 (10) (2018) 643–654.

[52] R.D. Ramirez, S. Sheridan, L. Girard, M. Sato, Y. Kim, J. Pollack, M. Peyton, Y. Zou, J.M. Kurie, J.M. DiMaio, Immortalization of human bronchial epithelial cells in the absence of viral oncoproteins, Cancer Res. 64 (24) (2004) 9027–9034.

[53] N.A.P. Franken, H.M. Rodermond, J. Stap, J. Haveman, C. van Bree, Clonogenic assay of cells *in vitro*, Nat. Protoc. 1 (5) (2006) 2315–2319.

[54] J.C. Mar, Y. Kimura, K. Schroder, K.M. Irvine, Y. Hayashizaki, H. Suzuki, D. Hume, J. Quackenbush, Data-driven normalization strategies for high-throughput quantitative RT-PCR, BMC Bioinformat. 10 (1) (2009) 110.

[55] J.T. Buijs, N.V. Henriquez, P.G. van Overveld, G. van der Horst, I. Que, R. Schwaninger, C. Rentsch, P. Ten Dijke, A.M. Cleton-Jansen, K. Driouch, R. Lidereau, R. Bachelier, S. Vukicevic, P. Clézardin, S.E. Papapoulos, M. G. Cecchini, C.W. Löwik, G. van der Pluijm, Bone morphogenetic protein 7 in the development and treatment of bone metastases from breast cancer, Cancer Res. 67 (18) (2007) 8742–8751.

[56] W. Li, H. Ma, J. Zhang, L. Zhu, C. Wang, Y. Yang, Unraveling the roles of CD44/CD24 and ALDH1 as cancer stem cell markers in tumorigenesis and metastasis, Sci. Rep. 7 (1) (2017) 13856.

[57] L. Walcher, A.-K. Kistenmacher, H. Suo, R. Kitte, S. Dluczek, A. Strauß, A.-R. Blaudszun, T. Yevsa, S. Fricke, U. Kossatz-Boehlert, Cancer stem cells—Origins and biomarkers: perspectives for targeted personalized therapies, Front. Immunol. 11 (2020) 1280.

[58] T. Blick, H. Hugo, E. Widodo, M. Waltham, C. Pinto, S.A. Mani, R.A. Weinberg, R. M. Neve, M.E. Lenburg, E.W. Thompson, Epithelial mesenchymal transition traits in human breast cancer cell lines parallel the CD44 hi/CD24 lo/-stem cell phenotype in human breast cancer, J. Mammary Gland Biol. Neoplasia 15 (2010) 235–252.

[59] S. Bhatia, J. Monkman, T. Blick, P.H. Duijf, S.H. Nagaraj, E.W. Thompson, Multi-omics characterization of the spontaneous mesenchymal–epithelial transition in the PMC42 breast cancer cell lines, J. Clin. Med. 8 (8) (2019) 1253.

[60] O. Delgado, A.A. Kaisani, M. Spinola, X.J. Xie, K.G. Batten, J.D. Minna, W. E. Wright, J.W. Shay, Multipotent capacity of immortalized human bronchial epithelial cells, PLoS One 6 (7) (2011) e22023.

[61] S. Bhatia, E.W. Thompson, J.H. Gunter, Studying the metabolism of epithelial-mesenchymal plasticity using the seahorse XFe96 extracellular flux analyzer, in: K. Campbell, E. Theveneau (Eds.), The Epithelial-to Mesenchymal Transition: Methods and Protocols, Springer US, New York, NY, 2021, pp. 327–340.

[62] B.Y. Oh, H.-T. Shin, J.W. Yun, K.-T. Kim, J. Kim, J.S. Bae, Y.B. Cho, W.Y. Lee, S. H. Yun, Y.A. Park, Y.H. Park, Y.-H. Im, J. Lee, J.-G. Joung, H.C. Kim, W.-Y. Park, Intratumor heterogeneity inferred from targeted deep sequencing as a prognostic indicator, Sci. Rep. 9 (1) (2019) 4542.

[63] A. Shukla, T.H.M. Nguyen, S.B. Moka, J.J. Ellis, J.P. Grady, H. Oey, A.S. Cristino, K. K. Khanna, D.P. Kroese, L. Krause, E. Dray, J.L. Fink, P.H.G. Duijf, Chromosome arm aneuploidies shape tumour evolution and drug response, Nat. Commun. 11 (1) (2020) 449.

[64] A. Sharma, E. Merritt, X. Hu, A. Cruz, C. Jiang, H. Sarkodie, Z. Zhou, J. Malhotra, G.M. Riedlinger, S. De, Non-genetic intra-tumor heterogeneity is a major predictor of phenotypic heterogeneity and ongoing evolutionary dynamics in lung tumors, Cell Rep. 29 (8) (2019) 2164–2174, e5.

[65] V.H. Teixeira, C.P. Pipinikas, A. Pennycuick, H. Lee-Six, D. Chandrasekharan, J. Beane, T.J. Morris, A. Karpathakis, A. Feber, C.E. Breeze, Deciphering the genomic, epigenomic, and transcriptomic landscapes of pre-invasive lung cancer lesions, Nat. Med. 25 (3) (2019) 517–525.

[66] A. Walens, J. Lin, J.S. Damrauer, B. McKinney, R. Lupo, R. Newcomb, D.B. Fox, N. W. Mabe, J. Gresham, Z. Sheng, A.B. Sibley, T. De Buysscher, H. Kelkar, P. A. Mieczkowski, K. Owzar, J.V. Alvarez, Adaptation and selection shape clonal evolution of tumors during residual disease and recurrence, Nat. Commun. 11 (1) (2020) 5017.

[67] B. Nguyen, C. Fong, A. Luthra, S.A. Smith, R.G. DiNatale, S. Nandakumar, H. Walch, W.K. Chatila, R. Madupuri, R. Kundra, C.M. Bielski, B. Mastrogiacomo, M.T.A. Donoghue, A. Boire, S. Chandarlapaty, K. Ganesh, J.J. Harding, C. A. Iacobuzio-Donahue, P. Razavi, E. Reznik, C.M. Rudin, D. Zamarin, W. Abida, G. K. Abou-Alfa, C. Aghajanian, A. Cercek, P. Chi, D. Feldman, A.L. Ho, G. Iyer, Y. Y. Janjigian, M. Morris, R.J. Motzer, E.M. O'Reilly, M.A. Postow, N.P. Raj, G. J. Riely, M.E. Robson, J.E. Rosenberg, A. Safonov, A.N. Shoushtari, W. Tap, M. Y. Teo, A.M. Varghese, M. Voss, R. Yaeger, M.G. Zauderer, N. Abu-Rustum,

J. Garcia-Aguilar, B. Bochner, A. Hakimi, W.R. Jarnagin, D.R. Jones, D. Molena, L. Morris, E. Rios-Doria, P. Russo, S. Singer, V.E. Strong, D. Chakravarty, L. H. Ellenson, A. Gopalan, J.S. Reis-Filho, B. Weigelt, M. Ladanyi, M. Gonen, S. P. Shah, J. Massague, J. Gao, A. Zehir, M.F. Berger, D.B. Solit, S.F. Bakhoum, F. Sanchez-Vega, N. Schultz, Genomic characterization of metastatic patterns from prospective clinical sequencing of 25,000 patients, Cell 185 (3) (2022) 563–575, e11.

[68] G. Malagoli Tagliazucchi, A.J. Wiecek, E. Withnell, M. Secrier, Genomic and microenvironmental heterogeneity shaping epithelial-to-mesenchymal trajectories in cancer, Nat. Commun. 14 (1) (2023) 789.

[69] A. Vasudevan, P.S. Baruah, J.C. Smith, Z. Wang, N.M. Sayles, P. Andrews, J. Kendall, J. Leu, N.K. Chunduri, D. Levy, Single-chromosomal gains can function as metastasis suppressors and promoters in colon cancer, Dev. Cell 52 (4) (2020) 413–428, e6.

[70] M. Saini, L. Schmidleitner, H.D. Moreno, E. Donato, M. Falcone, J.M. Bartsch, C. Klein, V. Vogel, R. Würth, N. Pfarr, E. Espinet, M. Lehmann, M. Königshoff, M. Reitberger, S. Haas, E. Graf, T. Schwarzmayr, T.-M. Strom, S. Spaich, M. Sütterlin, A. Schneeweiss, W. Weichert, G. Schotta, M. Reichert, N. Aceto, M. R. Sprick, A. Trumpp, C.H. Scheel, Resistance to mesenchymal reprogramming sustains clonal propagation in metastatic breast cancer, Cell Rep. 42 (6) (2023), 112533.

[71] R. Kasprowicz, R. Suman, P. O'Toole, Characterising live cell behaviour: traditional label-free and quantitative phase imaging approaches, Int. J. Biochem. Cell Biol. 84 (2017) 89–95.

[72] H. Zhou, D. Neelakantan, H.L. Ford, Clonal cooperativity in heterogenous cancers, Semin. Cell Dev. Biol. 64 (2017) 79–89.

[73] A.M. Martorana, G. Zheng, T.C. Crowe, R.L. O'Grady, J.G. Lyons, Epithelial cells up-regulate matrix metalloproteinases in cells within the same mammary carcinoma that have undergone an epithelial-mesenchymal transition, Cancer Res. 58 (21) (1998) 4970–4979.

[74] N. Stylianou, M.L. Lehman, C. Wang, A.T. Fard, A. Rockstroh, L. Fazli, L. Jovanovic, M. Ward, M.C. Sadowski, A.S. Kashyap, R. Buttyan, M.E. Gleave, T. F. Westbrook, E.D. Williams, J.H. Gunter, C.C. Nelson, B.G. Hollier, A molecular portrait of epithelial–mesenchymal plasticity in prostate cancer associated with clinical outcome, Oncogene 38 (7) (2019) 913–934.

[75] R.J. DeBerardinis, N.S. Chandel, Fundamentals of cancer metabolism, Sci. Adv. 2 (5) (2016), e1600200.

[76] L.G. Karacosta, B. Anchang, N. Ignatiadis, S.C. Kimmey, J.A. Benson, J.B. Shrager, R. Tibshirani, S.C. Bendall, S.K. Plevritis, Mapping lung cancer epithelial-mesenchymal transition states and trajectories with single-cell resolution, Nat. Commun. 10 (1) (2019) 5587.

[77] A. Goldman, B. Majumder, A. Dhawan, S. Ravi, D. Goldman, M. Kohandel, P. K. Majumder, S. Sengupta, Temporally sequenced anticancer drugs overcome adaptive resistance by targeting a vulnerable chemotherapy-induced phenotypic transition, Nat. Commun. 6 (1) (2015) 6139.

[78] A. Jaggupilli, E. Elkord, Significance of CD44 and CD24 as cancer stem cell markers: an enduring ambiguity, Clin. Dev. Immunol. 2012 (2012), 708036.

[79] M.B. Vaughan, R.D. Ramirez, W.E. Wright, J.D. Minna, J.W. Shay, A three-dimensional model of differentiation of immortalized human bronchial epithelial cells, Differentiation 74 (4) (2006) 141–148.

[80] M. Sato, M.B. Vaughan, L. Girard, M. Peyton, W. Lee, D.S. Shames, R.D. Ramirez, N. Sunaga, A.F. Gazdar, J.W. Shay, J.D. Minna, Multiple oncogenic changes (K-RAS (V12), p53 knockdown, mutant EGFRs, p16 bypass, telomerase) are not sufficient to confer a full malignant phenotype on human bronchial epithelial cells, Cancer Res. 66 (4) (2006) 2116–2128.